MAGNETIC RARE EARTH COMPOUNDS

Hewlett-Packard Company
Palo Alto, California 94304

SEMIANNUAL TECHNICAL REPORT

February 1972

Contract No. DAAH01-71-C-1259
Program Code No. 0D10

ARPA Support Office:
Research, Development, Engineering, and Missile Systems Laboratory
U.S. Army Missile Command
Redstone Arsenal, Alabama

A Research Project Sponsored by the Advanced Research Projects Agency, Department of Defense
Washington, D.C., ARPA Order No. 1642

NOTICE

"This research was sponsored by the Advanced Research Projects Agency of the Department of the Defense under ARPA Order 1627 and was monitored by the US Army Missile Command under Contract Number DAAH01-71-C-1259. Views and conclusions expressed herein are the primary responsibility of tne author or the contractor and should not be interpreted as representing the official opinion or policy of USAMICOM, ARPA, DOD or any other agency of the Government."

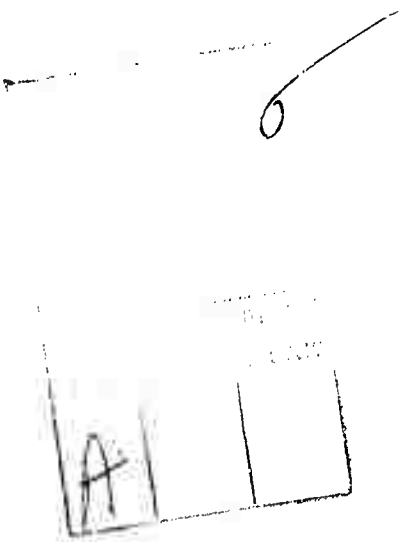

Unclassified
Security Classification

DOCUMENT CONTROL DATA - R&D

(Security classification of title, body of abstract and indexing annotation must be entered when the overall report is classified)

1. ORIGINATING ACTIVITY *(Corporate author)*

Hewlett-Packard Company
1501 Page Mill Road
Palo Alto, California 94304

2a. REPORT SECURITY CLASSIFICATION

Unclassified

2b. GROUP

3. REPORT TITLE

MAGNETIC RARE EARTH COMPOUNDS

4. DESCRIPTIVE NOTES *(Type of report and inclusive dates)*

Semiannual Technical Report (June 14, 1971 to December 14, 1971)

5. AUTHOR(S) *(Last name, first name, initial)*

Burmeister, Robert A.
Hiskes, Ronald

6. REPORT DATE	7a. TOTAL NO. OF PAGES	7b. NO. OF REFS
February 1972	61	20

8a. CONTRACT OR GRANT NO.

DAAH01-71-C-1259

b. PROJECT NO.

Technical Requirement No. 1335

c. Program Code No. 0D10

d. ARPA Order No. 1627

9a. ORIGINATOR'S REPORT NUMBER(S)

9b. OTHER REPORT NO(S) *(Any other numbers that may be assigned this report)*

10. DISTRIBUTION STATEMENT

Approved for public release; distribution unlimited.

11. SUPPLEMENTARY NOTES

12. SPONSORING MILITARY ACTIVITY

Advanced Research Projects Agency
Department of Defense,
Washington, D.C., ARPA Order 1627

13. ABSTRACT

Magnetically uniaxial rare earth garnets, such as $EuEr_2Ga_{0.7}Fe_{4.3}O_{12}$ and $Y_{1.3}GdYb_{0.7}Fe_{4.1}Ga_{0.9}O_{12}$, have been grown by quasi steady-state (isothermal) liquid phase epitaxial techniques. The epitaxial layers have been grown on Syton polished (111) $Gd_3Ga_5O_{12}$ substrates by the dipping technique in which the substrates, fastened to a platinum holder, are dipped into the supersaturated growth solution.

Both PbO-B_2O_3 and BaO-B_2O_3-BaF_2 solvents have been employed for the crystal growth, since each has certain distinct advantages and disadvantages for this type of growth situation. The BaO-based solvent has been characterized, and a solubility curve for a typical garnet, $EuEr_2Ga_{0.7}Fe_{4.3}O_{12}$, has been experimentally determined.

The magnetic films have been characterized with respect to solvent content and distribution coefficients of the constituent ions for each of the growth solutions, lattice parameter mismatch between epitaxial layer and substrate, and magnetic properties. Preliminary analyses indicate that the solvent impurity content is less than 0.05 wt. % for garnets grown in the BaO-based solvent compared to values up to 3 wt. % for those grown in PbO-based solvents, and that the distribution coefficients for the garnet constituents are much closer to unity for the former than for the latter solvent.

DD FORM 1 NOV 68 1473 REPLACES DD FORM 1473, 1 JAN 64, WHICH IS OBSOLETE FOR ARMY USE.

Unclassified
Security Classification

14. KEY WORDS	LINK A		LINK B		LINK C	
	ROLE	WT	ROLE	WT	ROLE	WT
Garnets						
Rare Earths						
Magnetic Bubbles						
Liquid Phase Epitaxy						
BaO-based Solvents						
Crystal Growth						

TECHNICAL REQUIREMENT NO. 1335
ARPA Order 1627

MAGNETIC RARE EARTH COMPOUNDS

SEMIANNUAL TECHNICAL REPORT

February 1972

HEWLETT-PACKARD
COMPANY
Palo Alto, California
94304
(415) 493-1501
Contract No. DAAH01-71-C-1259
Program Code No. OD10

Monitored By
ARPA Support Office
Research, Development, Engineering, and
Missile Systems Laboratory

Approved for Public Release
Distribution Unlimited

A Research Project Sponsored by the Advanced Research Projects Agency, Department of Defense, Washington, D.C., ARPA Order 1627

FOREWARD

This report describes work performed under Contract DAAH01-71-C-1259 for the ARPA Support Office, Research, Development, Engineering, and Missile Systems Laboratory, U.S. Army Missile Command, Redstone Arsenal, Alabama during the period June 14, 1971 through December 14, 1971. The monitor for this project was S. L. Johnston. The work was performed in the Solid-State Laboratory of Hewlett-Packard Laboratories under the direction of P. E. Greene. The work was supervised by R. A. Burmeister, and this report was written by R. Hiskes.

SUMMARY

Magnetically uniaxial rare earth garnets, such as $EuEr_2Ga_{0.7}Fe_{4.3}O_{12}$ and $Y_{1.3}GdYb_{0.7}Fe_{4.1}Ga_{0.9}O_{12}$, have been grown by quasi steady-state (isothermal) liquid phase epitaxial techniques. The epitaxial layers have been grown on Syton polished {111} $Gd_3Ga_5O_{12}$ substrates by the dipping technique in which the substrates, fastened to a platinum holder, are dipped into the supersaturated growth solution.

Both $PbO-B_2O_3$ and $BaO-B_2O_3-BaF_2$ solvents have been employed for the crystal growth, since each has certain distinct advantages and disadvantages for this type of growth situation. The BaO-based solvent has been characterized, and a solubility curve for a typical garnet, $EuEr_2Ga_{0.7}Fe_{4.3}O_{12}$, has been experimentally determined.

The magnetic films have been characterized with respect to solvent content and distribution coefficients of the constituent ions for each of the growth solutions, lattice parameter mismatch between epitaxial layer and substrate, and magnetic properties. Preliminary analyses indicate that the solvent impurity content is less than 0.05 wt. % for garnets grown in the BaO-based solvent compared to values up to 3 wt. % for those grown in PbO-based solvents, and that the distribution coefficients for the garnet constituents are much closer to unity for the former than for the latter solvent.

TABLE OF CONTENTS

TABLE OF CONTENTS

(Continued)

LIST OF ILLUSTRATIONS

LIST OF ILLUSTRATIONS

(Continued)

LIST OF TABLES

SECTION I

1.0. INTRODUCTION

Single-crystal rare-earth orthoferrites and mixed-cation garnets have become very important as hosts for a new class of high density information storage devices, the magnetic "bubble" memories, which utilize mobile cylindrical domains contained in thin films of these materials.[1] To ensure predictable response of the magnetic bubbles to applied magnetic forces, the films must be of uniform composition and thickness, and must be free of most common crystallographic imperfections. Epitaxial liquid phase and vapor phase growth techniques on nonmagnetic transparent substrates have proved successful in providing material meeting most of the device specifications of which a typical example is shown in Table I. Some important advantages of magnetic bubble memory devices are listed in Table II.

At this time, however, materials problems are still a major limitation to the practical utilization of bubble devices. In view of the technological importance of these devices and the key role of magnetic rare earth compounds, this program was undertaken in an effort to advance the state-of-the-art in the science and technology of these materials. The specific objectives of this program include the following:

1. Development of practical techniques for the growth of single crystals of rare earth compounds having properties suitable for studies and utilization of magnetic domain wall phenomena.
2. Acquisition of the necessary data to better characterize and quantitatively describe both the crystal growth process and the salient physical and chemical properties of the crystals produced.

TABLE I

Materials Specifications for Magnetic Bubble Memory Devices

D	6μ	Bubble Diameter
$4\pi M_s$	150 Gauss (±1% variation over the surface)	Saturation Magnetization
h	6μ (±1% variation over the surface)	Thickness
μ	> 200 cm/Oe-sec	Mobility
H_c	< 0.3 Oe	Coercive Force
Defect Density	< $5/cm^2$	Crystal defects which affect magnetic properties
H_k	> 1.5 · $(4\pi M_s)$	Anisotropy Field
$\left.\frac{dM_s}{dT}\right)_{298°K}$	<0.5 Oe/°K	Temperature coefficient of Magnetization

(Many of these specifications were listed in Reference 1.)

TABLE II

Advantages of Magnetic Bubble Devices

Memory and Logic in Same Material
Non-Destructive Read/Write
High Storage Density ($> 10^6$ bits/in^2)
Low Power Requirements
Radiation Hardness
Ability to Withstand High Gravitational Forces
Nonvolatility
Potential Resistance to Hostile EMI Environment with Appropriate Design
Unique Architecture
Portability
Low Cost
High Reliability over Long Time Periods (> 50 years)
Resistance to Mechanical and Vibration Damage
No Moving Parts

3. Determination of the relationships between methods and parameters of the crystal growth process and relevant physical properties of the crystals thus grown.

The choice of materials for the growth and characterization of the magnetic bubble materials has been dictated by current state-of-the-art knowledge of these materials. In the previous contract,[2] $YFeO_3$ was chosen as the initial material to be studied, since it is typical of the rare earth orthoferrites. Shortly after the initial reports of the possibility of preparing uniaxial garnet bubble materials, we initiated studies of the growth of these rare earth garnets, such as $Eu_2Er_1Ga_{0.7}Fe_{4.3}O_{12}$ and $Eu_1Er_2Ga_{0.7}Fe_{4.3}O_{12}$, which exhibit the necessary uniaxial anisotropy with a stable bubble size of 5-10 microns.[2]

In this program, we have investigated epitaxial growth of the rare earth garnets $EuEr_2Ga_{0.7}Fe_{4.3}O_{12}$ and $GdY_{1.3}Yb_{0.7}Ga_{0.9}Fe_{4.1}O_{12}$ on $Gd_3Ga_5O_{12}$ in both BaO-based and PbO-based solvents. The technique employed has been that of quasi steady-state liquid phase epitaxial solution growth, in which the solid-liquid interface is kept at a constant temperature during growth and the driving force for crystal growth is supersaturation at the interface. This crystal growth method alleviates the homogeneity problems found in the transient (cooling) techniques (particularly in the mixed cation rare earth garnets) and provides a means for reliable control of the parameters which enhance crystalline perfection.

SECTION II

2.0. CRYSTAL GROWTH

2.1. Introduction

Although rare earth orthoferrites and garnets have been grown by a variety of techniques,[3] the most promising method for the garnets has been that of epitaxial growth on a paramagnetic transparent substrate, including both liquid phase epitaxial (LPE)[4-8] and vapor phase epitaxial (VPE)[9-13] growth as shown in Table III. We have chosen LPE because it is an inherently simple and reliable process, one which provides optimum control of nucleation on a structurally similar substrate, and permits precise interface temperature and temperature gradient control when properly designed. The as-grown geometry (thin film on a supporting substrate)is ideal for device use, and the interface temperature is lower than that required for VPE, which minimizes thermal stress upon cooling to room temperature.

2.1.1. Liquid Phase Epitaxial Crystal Growth

The growth process is one of the most critical factors influencing the magnetic properties of the epitaxial layer. In order to maintain uniform magnetization and bubble diameter, variations in the layer thickness and composition excursions in directions both lateral and normal to the interface must be held to a minimum. Composition fluctuations normal to the interface can occur in one of two ways, (i) as a result of temperature fluctuations, since the distribution coefficient of each of the constituents is a function of temperature, or (ii) by depletion or enrichment of ions in the quiescent boundary layer adjacent to the growth interface if the growth time is short compared to the time required to reach a steady-state flux of ions through this boundary layer.[14]

TABLE III Magnetic Bubble Garnet Compositions Grown by Various Laboratories and Techniques

Garnet Composition †	Growth Technique	Growth Solution	Substrate	Lattice Parameter	Origin of Uniaxiality	Mobility Where Measured (cm/Oe-sec)	Magnetization ($4\pi M_s$)	Reference	Comm
$Er_2Tb_1Al_{1.1}Fe_{3.8}O_{12}$	Slow-cooled Solution Growth (bulk)	$PbO-B_2O_3$	"		Growth Induced	85	136	1	Type I cut
$Gd_{2.34}Tb_{0.66}Fe_5O_{12}$	"	"	"		"	120	137	1	Type II cut
$Gd_{0.95}Tb_{0.75}Er_{1.3}Al_{0.5}Fe_{4.8}O_{12}$	"	"	"		"	60	181	1	Type I cut
$Y_2Gd_1Al_{0.8}Fe_{4.2}O_{12}$	"	"	"		"	180	328	1	
$Y_{1.8}Eu_{0.2}Gd_{0.5}Tb_{0.5}Al_{0.6}Fe_{4.4}O_{12}$	"	"	"		"	186	450	1	
$Eu_{0.09}Gd_{2.32}Tb_{0.59}Fe_5O_{12}$	"	$PbO-B_2O_2$ and	"		"	-	-	2	Type II cut
$Eu_{0.09}Gd_{2.32}Tb_{0.59}Fe_5O_{12}$	"	$BaO-BaF_2-B_2O_3$			"			HPL	
$Eu_2ErGe_{0.7}Fe_{4.3}O_{12}$	"	"	"		"	165	196	1	Type I cut
$Eu_2ErGe_{0.7}Fe_{4.3}O_{12}$	LPE	$PbO-B_2O_3$ and	$Gd_3Ga_5O_{12}$		"	-	173	2	Grown on {110} $Gd_3Ga_5O_{12}$
$EuEr_2Ga_{0.7}Fe_{4.3}O_{12}$	LPE	$BaO-BaF_2-B_2O_3$			"			HPL	
$EuEr_2Ge_{0.7}Fe_{4.3}O_{12}$	LPE	$PbO-B_2O_3$ and	$Gd_3Ge_5O_{12}$		"		170	3	
$Eu_2ErGa_{0.7}Fe_{4.3}O_{12}$	"	$BaO-BaF_2-B_2O_3$			"			HPL	
$Gd_{0.5}Y_{2.5}Fe_4Ge_1O_{12}$	LPE	$PbO-B_2O_3$	$Gd_3Ga_5O_{12}$		Stress Induced	-	150	4	High defect density
$Eu_{0.5}Y_{2.5}Fe_4Ga_1O_{12}$	LPE	$PbO-B_2O_3$	"		"	-	280	4	"
$Tb_{2.5}Er_{0.5}Fe_5O_{12}$	CVD	-	$Sm_3Ge_5O_{12}$		Stress Induced (ion implantation)	-	-	5	Film was cracked
$Eu_{1.75}Er_{1.25}Fe_{4.1}Al_{0.8}O_{12}$	LPE	$PbO-B_2O_3$	$Gd_3Ge_5O_{12}$		Stress Induced (ion implantation)	90	-	6	
$Y_3Ge_{0.5}Fe_{2.5}O_{12}$	CVD	-	$Dy_{0.75}Gd_{2.25}Ga_5O_{12}$		Stress Induced	-		5	
$Y_3Ge_{0.8}Fe_{4.2}O_{12}$	Slow-cooled Solution Growth (bulk)	$PbO-B_2O_3$ PbF_2	"		Stress Induced	-	840	7	Cut from bulk crystal, then
$Y_3Ge_{1.0}Fe_{4.0}O_{12}$	"	"	"		"	-	320	6	"
$Y_3Ge_{1.3}Fe_{3.7}O_{12}$	"	"	"		"	-	45	6	"
$Y_3Ge_{1.5}Fe_{3.5}O_{12}$	"	"	"	12.356	"	>2000	40	7	"
$Y_3Ge_{1.7}Fe_{3.3}O_{12}$	"	"	"		"	-	69	6	"
$Gd_{1.5}Y_{1.5}Al_{0.5}Fe_{4.5}O_{12}$	Slow-cooled solution Growth	$PbO-B_2O_3PbF_2$	-	12.380	Stress Induced	>2000	316	7	Cut from bulk crystal, then
$Gd_{0.88}Y_{1.28}Yb_{0.73}Ge_{0.92}Fe_{4.68}O_{12}$	"	"	"	12.375	"	720	124	"	"
$GdY_{1.2}Yb_{0.7}Ge_{0.8}Fe_{4.1}O_{12}$	"	"	"	12.375	"	520	121	"	"
$Sm_{0.37}Gd_2Dy_{0.62}Fe_5O_{12}$	"	"	"	12.471	"	>2000	240	"	"
$Sm_{1.1}Dy_{1.9}Ge_{0.8}Fe_{4.2}O_{12}$	"	"	"	12.442	"	24	128	"	"
$Sm_{0.1}Gd_{2.34}Tb_{0.66}Fe_5O_{12}$	"	"	"	-	"	-	230	"	"

TABLE III Magnetic Bubble Garnet Compositions Grown by Various Laboratories and Techniques

Garnet Composition	Growth Technique	Growth Solution	Substrate	Lattice Parameter	Origin of Uniaxiality	Mobility Where Measured (cm/Oe-sec)	Magnetization ($4\pi M_s$)	Reference	Com
$Sm_{0.6}Dy_{1.2}Y_{0.8}Fe_{4.1}Ga_{0.2}O_{12}$	"	"	"	"	"	"	28	"	"
$Y_3Ga_{1.2}Fe_{3.2}O_{12}$	CVD	"	$Gd_3Ga_5O_{12}$	12.327	Stress Induced	1800		8	Crazed film
"	"	"	$Dy_xGd_{3-x}Ga_5O_{12}$	12.387	"	"	"	8	No cracking
$Er_3Ga_{0.6}Fe_{4.4}O_{12}$	"	"	$Dy_xGd_{3-x}Ga_5O_{12}$	12.381	"	222	300	8	Crazed
$Gd_{3-x}Tb_xFe_2O_{12}$	LPE	Bi_2O_3-V_2O_5	$Nd_3Ga_5O_{12}$	"	Growth Induced	"	"	10	No data give
$Y_{3-x}Gd_xFe_5O_{12}$	LPE	Bi_2O_3-V_2O_5	$Gd_3Ga_5O_{12}$	"	Growth Induced	"	"	10	No data give
$Y_{0.84}Ga_{1.07}Yb_{0.37}La_{0.42}Al_{0.7}Fe_{4.2}O_{12}$	LPE	PbO-B_2O_5	$Gd_3Ga_5O_{12}$		Growth and Stress Induced	273	240	10	Circuit operation achie
$Y_{1.3}Gd_{0.7}Yb_{0.7}Ga_{0.1}Fe_{4.9}O_{12}$	LPE	"	"		"	830	121	"	"
$Y_{1.3}Gd_{0.7}Yb_{0.7}Ga_{0.1}Fe_{4.9}O_{12}$	LPE	"	"		"			HPL	
$Er_{1.99}Gd_{1.01}Ga_{0.22}Fe_{4.78}O_{12}$	LPE	"	"		"	89	143	11	
$Ca_{1.9}Si_{1.1}V_{0.95}Fe_{4.05}O_{12}$	Slow cooled solution growth (bulk)	PbO-B_2O_3		2.532	Growth Induced	1100	26	11	

†In many cases these compositions are nominal and relate only to the solution composition.

The need for compositional control suggests isothermal growth by either the steady-state growth process in which nutrients are transported down a temperature gradient to the growing crystal or by a quasi-steady state approach in which the entire growth solution is initially supercooled and then maintained at constant temperature during growth. The steady-state technique is the most controllable, but for the rapid growth velocity ($\gtrsim 10^{-6}$cm/sec) and short growth times (10 min.) needed for heteroepitaxial garnet growth, most of the growth occurs during the initial transient before true steady-state can be achieved, and therefore, in this portion of the contract period, the quasi steady-state mode has been employed.

2.1.2. Garnet Composition and Substrate Selection

Garnet compositions must be carefully selected to meet the stringent materials requirements listed in Table I, and perhaps the most critical control is needed in matching substrate and epitaxial layer lattice parameters. This match has in some cases been met by forming solid solutions, such as $Gd_3Ga_5O_{12}$ with either $Nd_3Ga_5O_{12}$, $Sm_3Ga_5O_{12}$, or $Dy_3Ga_5O_{12}$ as shown in Figure 1 to raise or lower the lattice parameter of the substrate respectively, but the majority of the bubble garnets have been grown on $Gd_3Ga_5O_{12}$ (see Table III).

From the numerous compositions shown in Table III (which indeed represent a fraction of the possible usable compositional combinations), we have chosen to concentrate on two, $EuEr_2Ga_{0.7}Fe_{4.3}O_{12}$ and more recently $GdY_{1.3}Yb_{0.7}Fe_{4.1}Ga_{0.4}O_{12}$ for several reasons; (i) they exhibit mobile bubble domains at reasonable values of magnetic bias and drive fields, (ii) they are among the most thoroughly studied of the garnets in Table III, and therefore, the most amenable to further analysis, particularly as a means for evaluating solvent performance in the case of the BaO-based solvent, (iii) they can be grown on $Gd_3Ga_5O_{12}$ substrates, which are available in large quantities and can be processed to the surface perfection necessary for epitaxial growth, and (iv) these combinations of epitaxial layers and substrate are representative of the rare earth bubble garnet growth process. The evaluation of techniques for proper growth and characterization of these garnets is germane to the entire class of rare earth garnets, and attention can thus be shifted to any other compositions deemed more desirable at any point in the program without loss of continuity to the project.

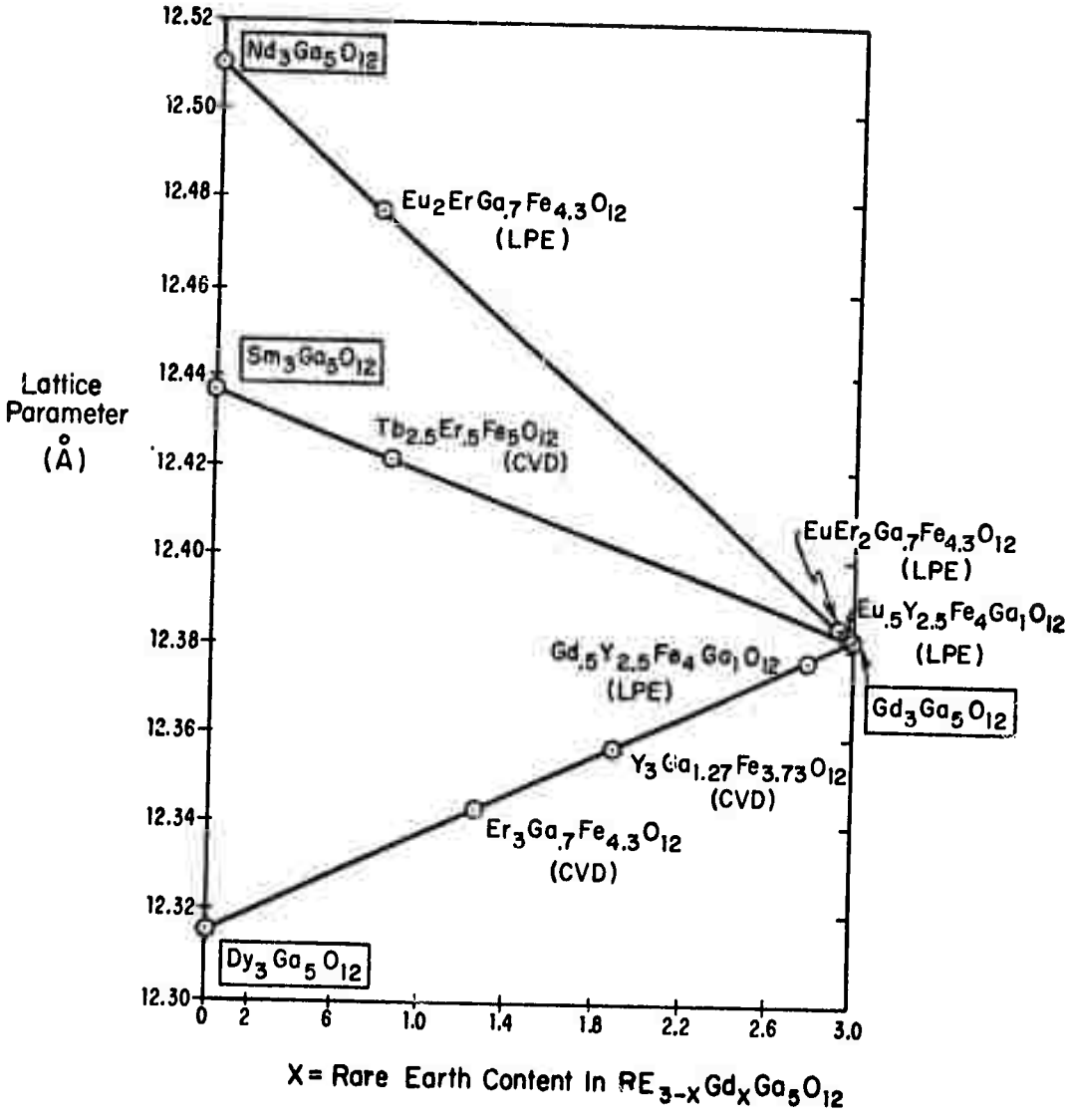

Figure 1. Lattice Parameter Match Between Substrates and Magnetic Garnets.

2.1.3. Solvent Requirements

There are certain basic solvent requirements needed for solution crystal growth which are enumerated below:

1. Low vapor or dissociation pressure and low reactivity with the crucible at crystal growth temperatures is desirable, in order to avoid changes in liquid level and composition.
2. The solvent should have a lower density than the crystals being grown in it so that any crystals which nucleate randomly will sink to the bottom of the crucible where they will not interfere with growth on the substrate.
3. The solvent should have a high solubility for the crystal growth constituents, and the metastable supercooled solution should be stable up to 50°C supercooling for heteroepitaxial growth.
4. The solubility curve (temperature versus composition) should be steep to permit precise control of supersaturation by controlling the solution temperature.
5. The distribution coefficients of the crystal constituents should not vary with temperature to prevent spurious composition fluctuations due to temperature excursions in the solution during growth.
6. The distribution coefficients as well as the solubility of the solvent ions in the crystal must be very low to prevent solvent incorporation during growth. This effect can be quite serious and has been found to lead to nonstoichiometry and large lattice parameter changes in the garnet epitaxial layer.[8]

7. It is desirable for the compound to be congruently saturating to enhance stoichiometric growth and deter the formation of other phases.
8. The solvent should have both a low melting point and low viscosity to permit growth at as low a temperature as possible.
9. The solvent must wet the substrate and growing crystal, but should also readily run off as the crystal is pulled out of the solution after growth.
10. The solution should be readily soluble in common solvents that do not attack the crystal or the growth crucible to facilitate cleaning operations.
11. The solvent should be inexpensive and readily obtainable in high purity form.

Although there is no universal solvent which satisfies all these requirements even for a restricted class of compounds such as the rare earth garnets, it is desirable to tailor the solvent to the crystal being grown to satisfy as many of the requirements as possible. In this program we are evaluating two classes of solvents, the PbO-based and the BaO-based solvents. The commonly used PbO-B_2O_3 solvents fail in requirements 1, 2, 5, 6, and 7. The BaO-based solvents, on the other hand, fulfill requirements 1-7 as well as 10 and 11. Only in requirements 8 and 9 are they surpassed by the PbO-based solvents as will be discussed more fully in subsequent sections of this report.

2.2. Experimental Procedures

2.2.1. Characterization of the $BaO-BaF_2-B_2O_3$ Solvent

Many of the properties of this solvent have been discussed previously.[2] In this report period interest centered on the solubility of the rare earth garnets as well as the optimum solvent composition for crystal growth of the garnets. The phase diagram has been explored in more detail as shown in Figure 2. The best results to date have been obtained with the composition 41 (mole)% BaO, 41% B_2O_3 and 18% BaF_2, which was used as well for the growth of the orthoferrites in the first phase of this contract.

The data in Figure 2 were obtained by cooling various solvent compositions to the temperature at which a large increase in viscosity was noted by the difficulty with which a platinum stirring rod could be moved through the solution. The utility of the solvent was limited by the fact that at temperatures below 850°C the viscosity was found to increase with time, and the data given pertain to times of the order of 10-30 minutes, which are representative of the actual crystal growth times. At longer times (several hours), the initially fluid compositions often almost completely solidified. Figure 2 thus reflects solvent properties for a dynamic crystal growth situation rather than the equilibrium properties of the solution.

The compositions along the $BaO-BaF_2$ binary were found to readily attack the platinum crucible at temperatures exceeding 1000°C (as determined by a darkening of the interior surface of the crucibles detected after the solution was removed and by 1-2 wt. % platinum found in the solution by emission spectrographic analysis after three days at 1050°C). These

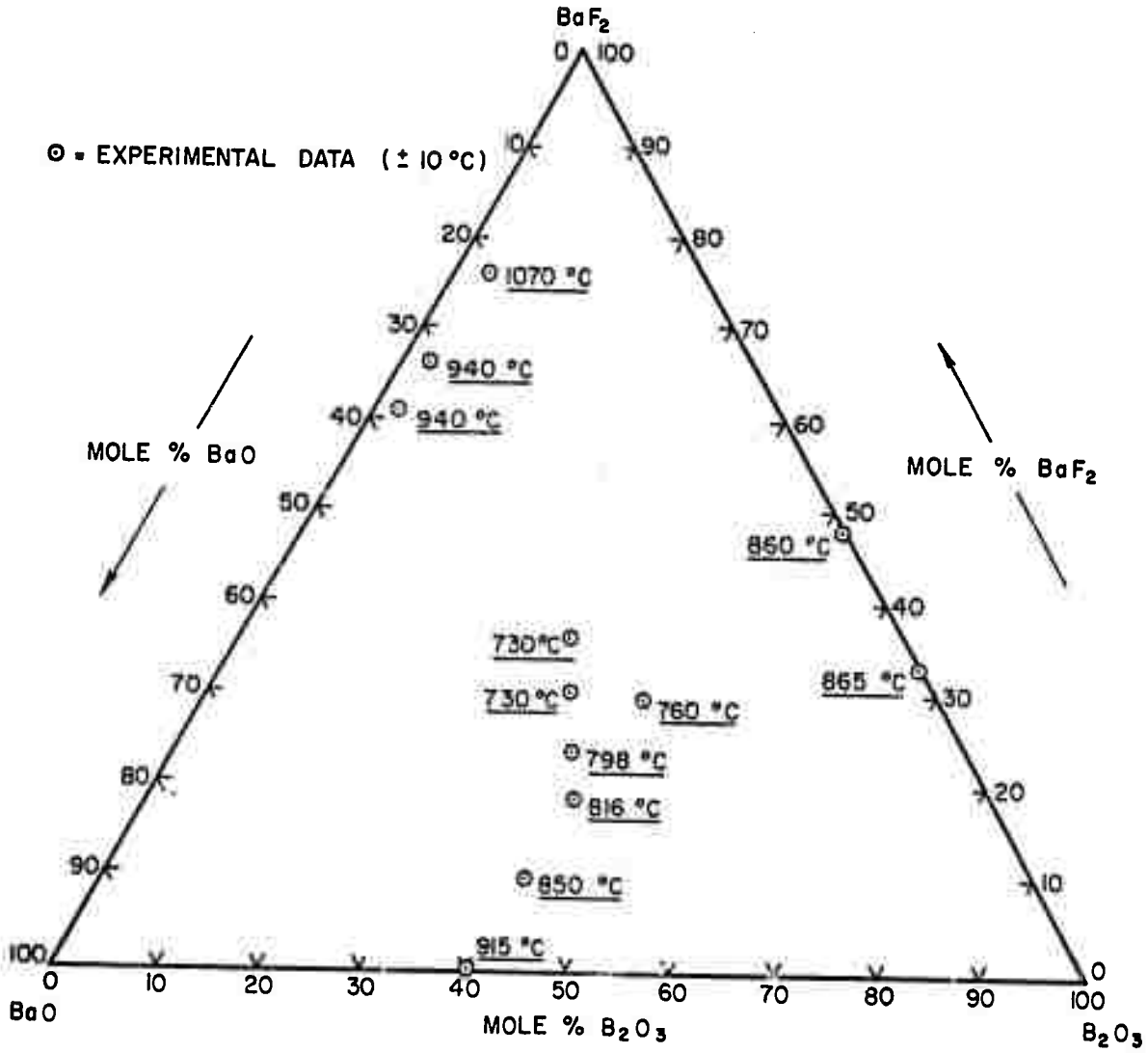

Figure 2. Approximate Liquidus Points for the $BaO-B_2O_3-BaF_2$ System (the points represent approximate temperatures at which a large qualitative increase in viscosity was noted).

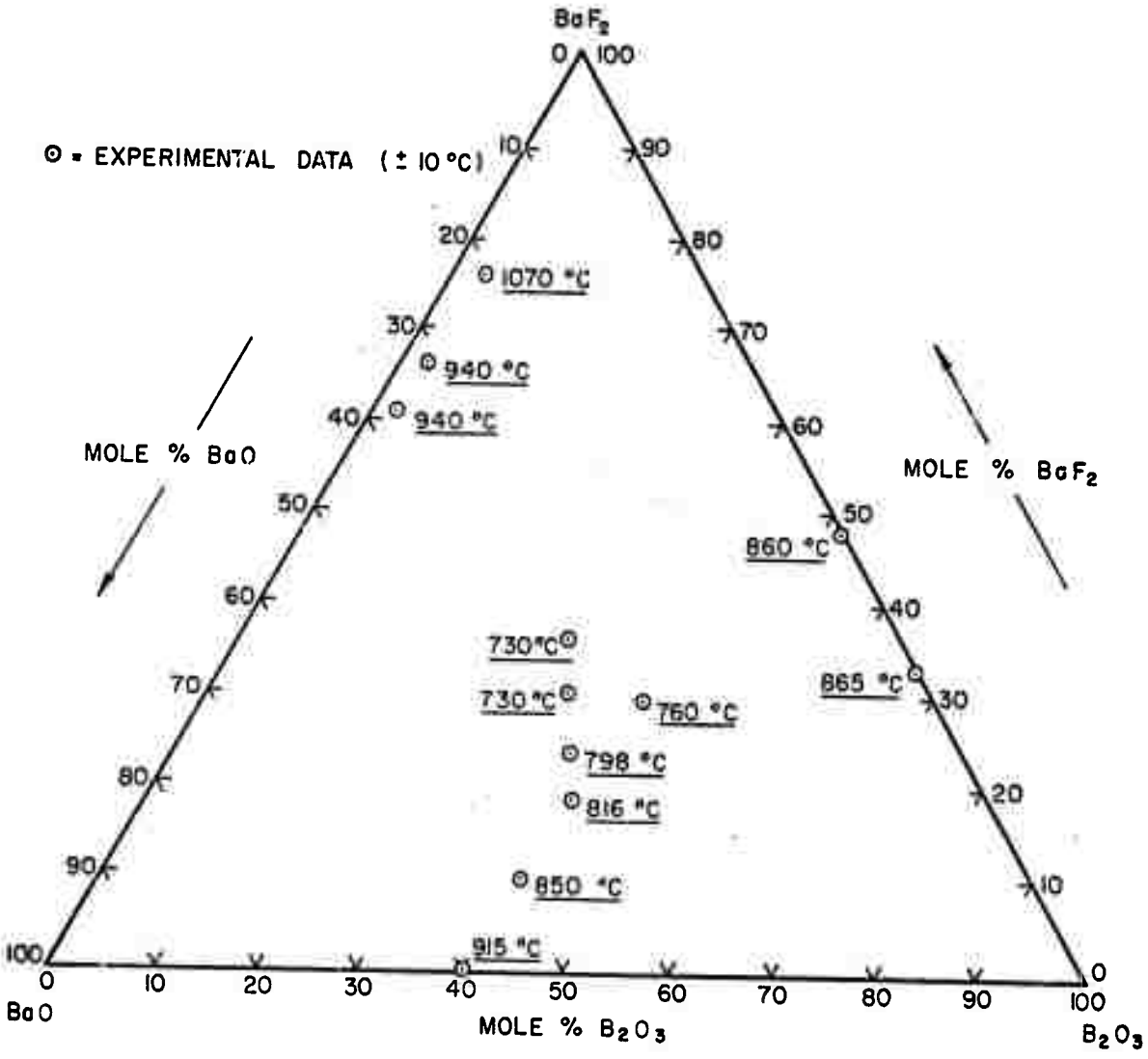

Figure 2. Approximate Liquidus Points for the BaO-B_2O_3-BaF_2 System (the points represent approximate temperatures at which a large qualitative increase in viscosity was noted).

2.2. Experimental Procedures

2.2.1. Characterization of the $BaO-BaF_2-B_2O_3$ Solvent

Many of the properties of this solvent have been discussed previously.[2] In this report period interest centered on the solubility of the rare earth garnets as well as the optimum solvent composition for crystal growth of the garnets. The phase diagram has been explored in more detail as shown in Figure 2. The best results to date have been obtained with the composition 41 (mole)% BaO, 41% B_2O_3 and 18% BaF_2, which was used as well for the growth of the orthoferrites in the first phase of this contract.

The data in Figure 2 were obtained by cooling various solvent compositions to the temperature at which a large increase in viscosity was noted by the difficulty with which a platinum stirring rod could be moved through the solution. The utility of the solvent was limited by the fact that at temperatures below 850°C the viscosity was found to increase with time, and the data given pertain to times of the order of 10-30 minutes, which are representative of the actual crystal growth times. At longer times (several hours), the initially fluid compositions often almost completely solidified. Figure 2 thus reflects solvent properties for a dynamic crystal growth situation rather than the equilibrium properties of the solution.

The compositions along the $BaO-BaF_2$ binary were found to readily attack the platinum crucible at temperatures exceeding 1000°C (as determined by a darkening of the interior surface of the crucibles detected after the solution was removed and by 1-2 wt. % platinum found in the solution by emission spectrographic analysis after three days at 1050°C). These

compositions, even though relatively low melting, were considered unsuitable for crystal growth. The solutions along the BaF_2-B_2O_3 binary did not produce the garnet phase on the substrate after exploratory crystal growth from a congruent solution at 800-900°C. Other phases present were not identified but were presumed to be fluorides, and resulting crystals were small colorless whiskers.

After selecting the appropriate solvent composition, the proper rare earth concentration in the solute was determined. It had been found in the PbO-based solvents that the equilibrium phase field for the garnet lies far to the iron rich side of the stoichiometric rare earth composition (37.5 mole %), and that epitaxial films containing fewest defects are produced when the rare earth concentration in the solute is ~ 7 mole %.[4] On the other hand, yttrium iron garnet had been found to be congruently saturating by Linares,[16] and we found that indeed the rare earth garnets could be grown from a stoichiometric garnet composition. In fact, when using the 7 % rare earth solute composition in the BaO-based solvent, large quantities of reddish hexagonal crystals appeared, which were deduced by X-ray (Debye-Scherrer) analysis to be a gallium substituted barium ferrite. Compositions in this range were also very high melting, often solidifying at temperatures approaching 1050°C for a 20.3 mole% garnet solution. The solution exhibiting highest melt fluidity and garnet solubility consisted of 42.5 mole% rare earths- 57.5% (iron + gallium), slightly toward the orthoferrite side of the stoichiometric garnet composition.

An approximate solubility curve for liquid phase epitaxial growth was determined for this combination of solute and solvent by suspending a polished $Gd_3Ga_5O_{12}$ substrate in the solution at various temperatures for twenty minutes, and noting the highest temperature at which growth occurred on the substrate. Growth was easily detectable because even an extremely thin (<1μ) epitaxial layer of $EuEr_2Ga_{0.7}Fe_{4.3}O_{12}$ produced the typical green coloration on the colorless substrate. The experimental solubility curve obtained in this fashion is shown in Figure 3. Since a saturation temperature of ~970°C has been reported for 9.7 mole% $EuEr_2Ga_{0.7}Fe_{4.3}O_{12}$ in the $PbO-B_2O_3$ solvent,[17] Figure 3 indicates this garnet is nearly twice as soluble in the BaO-based solvent at this temperature.

2.2.2. Substrate Preparation and Evaluation

2.2.2.1. Initial Garnet Boule Preparation

Substrate material acquired in boule form was sawed into 0.5 mm thick wafers with an annular (I. D.) saw fitted with a diamond impregnated blade. An overall surface flatness of ±5μ with the deepest microgrooves <2μ was determined by profilometer measurements.

2.2.2.2. Substrate Processing

A process was developed which routinely produces flat surfaces having no surface damage on 1/2 - 1 1/16" diameter $Gd_3Ga_5O_{12}$ substrates. The surfaces are first lapped with 3μ alumina, primarily to flatten the substrate surface, but also to remove the last trace of saw damage or any heavy damage which the substrate may have incurred during handling. The

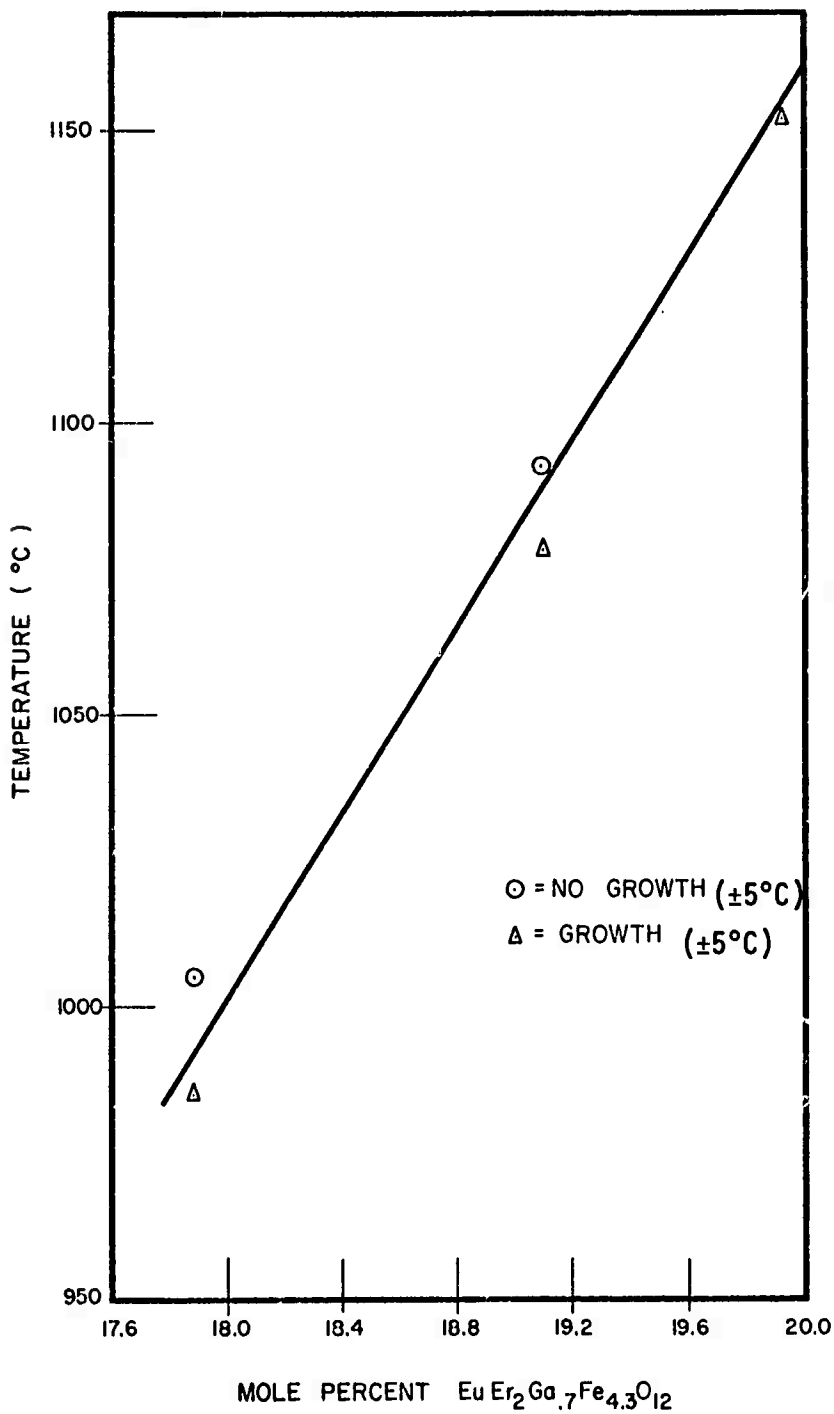

Figure 3. Approximate Solubility Curve for $EuEr_2Ga_{0.7}Fe_{4.3}O_{12}$ in 41 (mole)% BaO, 41% B_2O_3, 18% BaF_2.

amount of material removed in this step depends on the history of the individual substrate, but is generally 5-6μ . After lapping, the substrate surface is prepolished with 1μ diamond grit on a nylon pad, and approximately 12μ of material is removed to eliminate all lapping damage. The final polishing is done by a colloidal suspension of silica particles (400Å diam.) in a caustic solution (Syton*). Figure 4 illustrates the polishing rate for one of the pads used in the final polishing step.

A 1940 gm/cm^2 load results in a $Gd_3Ga_5O_{12}$ stock removal rate of 16μ /hr. which produces flat damage-free surfaces (see Section 2.2.2.3 for surface evaluation). After each step in the processing, the thickness of the substrate is measured by lowering the needle sensor of an electronic thickness measuring instrument onto the surface of the substrate, which applies a force of 2.5 gm on the point of contact at the surface.

2.2.2.3. Evaluation of Substrate Surface Preparation

To determine whether the surface preparation was adequate to remove all of the scratches in the final polishing step, the substrates are etched in 85% H_3PO_4 for three minutes at 160°C. This selective etchant readily removes damaged or any other highly strained regions, thus delineating scratches and etch pits. Experience with this etchant has shown that it reveals very slight mechanical damage and that it provides a useful test for determining the suitability of a substrate surface for epitaxial growth.

*A trade name for a product of the Monsanto Corporation.

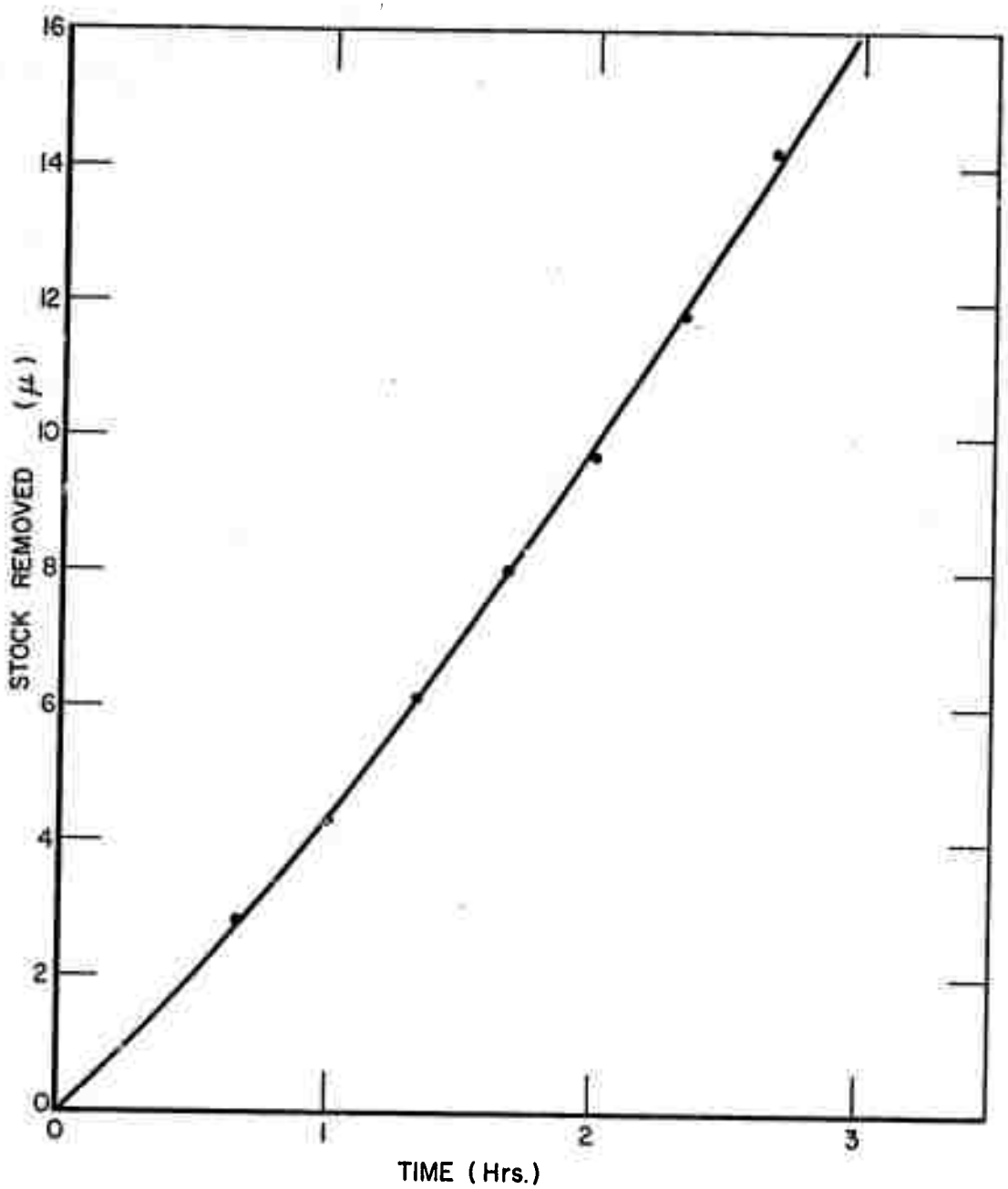

Figure 4. $Gd_3Ga_5O_{12}$ Stock Removal Produced by Syton Polishing.

2.2.2.4. Substrate Characterization and Evaluation

There are a number of substrate properties which influence epitaxial growth on the substrate, including lattice parameter, orientation and thickness. Substrate defects, such as dislocations, inclusions, inhomogeneous strain and growth striations, which are related to the Czochralski growth process, can also cause large fluctuations in the local coercive force in the epitaxial layers.

In order to understand the interaction between substrate parameters and epitaxial layer perfection, the following techniques have been used to characterize the substrates;

1. Lattice parameters of $Gd_3Ga_5O_{12}$ substrates have been determined by Debye-Scherrer and single crystal X-ray diffractometry techniques. Details and results of these analyses are given in Section 3.2.
2. Substrate orientation was determined by the Laue X-ray diffraction technique to be {111} ±1.5°.
3. Selective etching has been used for the detection of residual mechanical polishing damage and delineation of dislocations. 85% orthophosphoric acid and a mixture of 50% (by volume) orthophosphoric and 50% sulfuric acid have been used. Examples of etch pits produced in this fashion are shown in Figures 5 and 6. Two distinct etch pit morphologies are shown in Figure 6, which may be caused by differences in dislocation orientation.
4. Inhomogenous strain in the substrates was detected by transmission microscopy using polarized light.

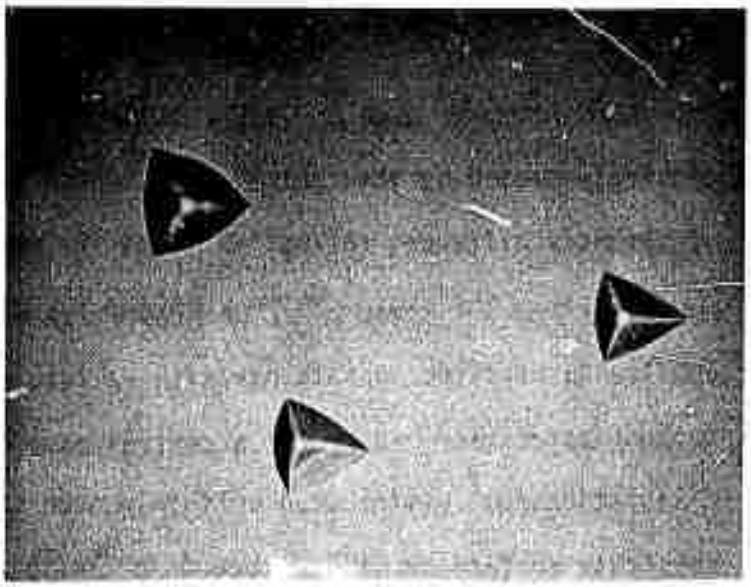

Figure 5. Etch Pits near the Perimeter of a {111} $Gd_3Ga_5O_{12}$ Substrate Containing a Core Defect (500X).

Figure 6. Etch Pits in a {111} $Gd_3Ga_5O_{12}$ Substrate Containing No Core Defect (1600X).

This technique was used primarily to determine the extent of strain caused by the central core, which is a region of slightly different refractive index in the substrate caused by faceted growth. (See Figure 7.)

Substrates received to date have fallen into one of two categories; either having (i) a central core defect with 0-10 dislocations/cm^2 distributed uniformly over the entire substrate surface or (ii)no core defect with a dislocation density greater than $10^3/cm^2$, inhomogeneously distributed in small clusters in the interior and around the periphery of the substrates.

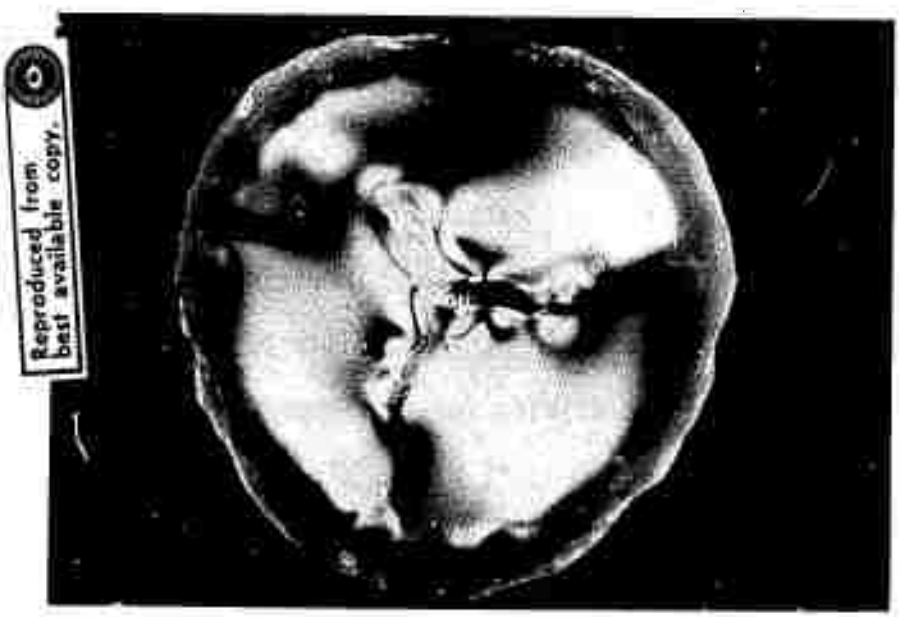

Figure 7. Strain Associated with Core Defect in $Gd_3Ga_5O_{12}$ Boule (polarized transmitted light, 3X).

2.2.3. Experimental Crystal Growth

2.2.3.1. Growth in BaO-based Solvents

$EuEr_2Ga_{0.7}Fe_{4.3}O_{12}$ and $Eu_2ErGa_{0.7}Fe_{4.3}O_{12}$ were grown in several different compositions of the BaO-based solvent by the isothermal quasi-steady-state LPE technique as well as the rapid cooling LPE method.[4] The compositions employed were:

i. 34.80 (mole) % BaO
34.80% B_3O_3
30.40% BaF_2

ii. 47.49% BaF_2
52.51% B_2O_3

iii. 41% BaO
41% B_2O_3
18% BaF_2 .

The (Eu, Er)/(Fe, Ga, Eu, Er) ratio in the solution was varied from 10.18 mole% (far to the iron rich side of the stoichiometric composition) to 42.5 mole % rare earth content to determine the stability region for garnet growth. Since no solubility data existed for this growth system, the solute concentration was varied systematically from 13.9 mole % to 20.3 mole % and the growth temperature varied from 860°C to 1100°C in order to determine the optimum growth conditions. In all cases, the solution was initially held at 1200-1300°C for 6-24 hours to ensure dissolution of all garnet constituents, and then held at 1050-1150°C for 12 hours before quickly cooling to the growth temperature for each run. A maximum of 9 runs were made from each new batch of growth solution, and a typical composition is BaO 38.1 gm, B_2O_3 17.2 gm, BaF_2 19.0 gm, Er_2O_3 15.8 gm, Eu_2O_3 6.7 gm, Fe_2O_3 11.2 gm and Ga_2O_3 2.1 gm.

In all cases the dipping technique of LPE growth was used.[4] For some of the earlier runs, the $Gd_3Ga_5O_{12}$ substrates were polished on only one side and were clamped to a platinum sheet, but the substrate holder was subsequently modified to one very similar to the wire holder shown in Figure 8, and substrates polished on both sides were used. The holder was then modified once again for the later runs to a simple platinum loop passing through a hole drilled into the substrate (see Figure 12) in order to minimize the amount of contact between substrate and substrate holder, primarily to enhance solvent runoff after crystal growth. These approaches are simple to implement but are relatively crude, and problems arise because of a different thermal environment in the vicinity of the holder, boundary layer pertubations near the holder, and solvent adhesion at the holder - substrate junction (caused by surface tension effects) after growth. A much more satisfactory type of holder, which was used in the preceding contract period and is presently being explored for garnet growth, is a holder such as that shown in Figure 9, which completely exposes the surface of the substrate (held horizontally) to the growth solution, which incorporates capability for rotation of the substrate and the introduction of a temperature gradient across the substrate normal to the liquid-solid interface.

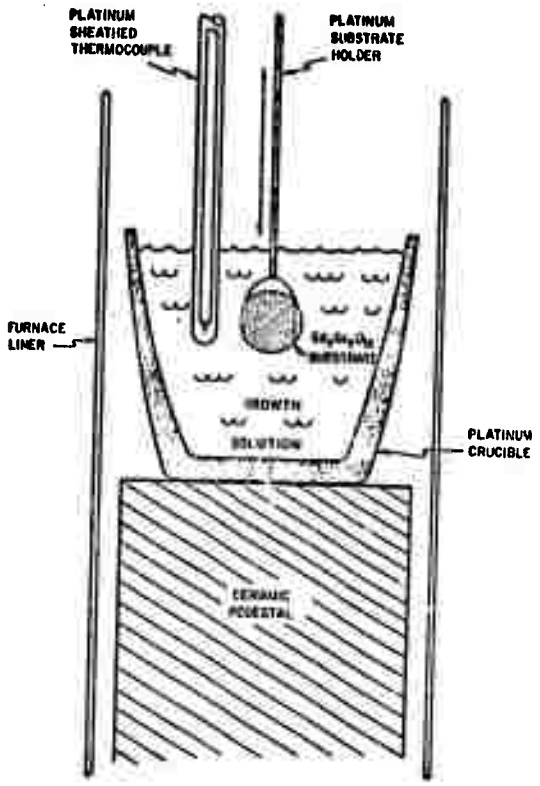

Figure 8. Apparatus for Epitaxial Crystal Growth of Magnetic Bubble Garnet.

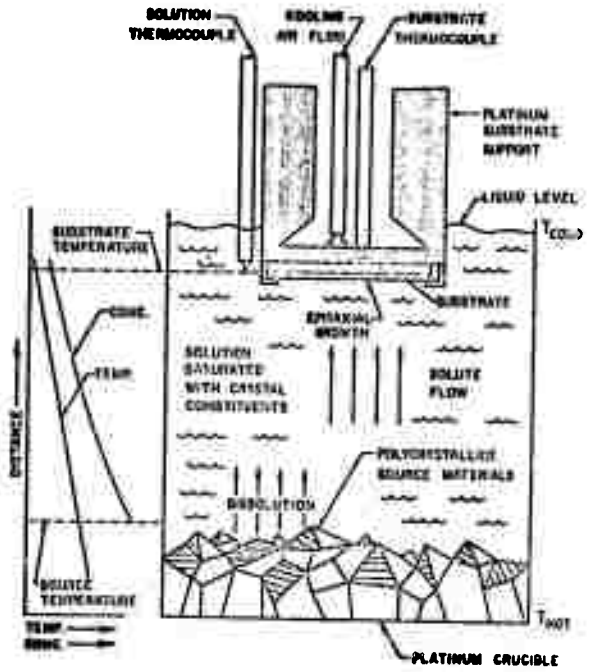

Figure 9. Steady-State Liquid Phase Epitaxial Growth Apparatus.

2.2.3.1.1. Results and Discussion of Growth in BaO-based Solvents

The growth parameters for typical LPE growth runs of $EuEr_2Ga_{0.7}Fe_{4.3}O_{12}$ in the BaO-based solvent are shown in Table IV. For rare earth concentrations in the solution less than the stoichiometric 37.5 mole %, there were usually red hexagonal platelets that had grown in and on the epitaxial layer, indicating competing growth of a solid solution of barium (iron, gallium) ferrite. The presence of 20.3 mole % solute at rare earth concentrations of 10-15 mole % raised the solidification temperature of the solvent from the 730°C range shown in Figure 2 to nearly 1050°C, indicating that the solvus surface of the phase diagram rises very steeply in this region. Conversely, solute compositions containing up to 42.5% rare earths were quite fluid at this temperature, and no evidence of the orthoferrite phase was detected on epitaxial layers grown in this region of the phase diagram, indicating that the garnet phase is quite stable here. Since the garnet was found to be congruently saturating in the $BaO-B_2O_3$ solvent by Linares,[16] it is probably congruently saturating in this solvent also, hence the highest point in the liquidus surface in the vicinity of stoichiometry may be expected at or very close to the stoichiometric composition. In order to grow at the lowest possible temperature (as well as to maintain the greatest possible solution fluidity) we chose the presumed valley in the liquidus surface at the iron-rich side of stoichiometry (~ 42.5%) as the best crystal growth composition. The solubility curve shown in Figure 3 pertains to this composition, and the best epitaxial layers thus far have been grown from this solution composition.

TABLE IV

Growth Parameters for LPE Garnet Growth in $BaO-B_2O_3-BaF_2$ Solvents

Run No.	Solvent Composition (mole %)	Solute Concentration (mole %)	Rare Earth Concentration	Soak and Run Temp. (°C)	Time or Cooling Rate	Remarks
LS25	34.80 BaO, 34.80 B_2O_3 30.40 BaF_2	23.5%	10.2%	S 1215 R 1200→1150	3.8°C/min.	Very little growth (<1μ)
LS45	47.5 BaF_2, 52.5 B_2O_3	13.9%	36.5	S 1050 R 900→865	4.25°C/min.	No growth
LS48	47.5 BaO, 52.5 B_2O_3	15.7%	37.5	S 1050 R 861	6 hour	No growth
LS53	41 BaO, 41 B_2O_3 18 BaF_2	20.3%	42.5	S 1170 R 947	20 min.	12μ layer
LS54	"	"	"	S 1170 R 957	5 min.	6μ layer
LS55	"	"	"	S 1150 R 853	15 min.	10μ layer
LS57	"	"	"	S 1143 R 997	10 min.	2μ layer
LS63	"	"	"	S 1154 R 1092.3 - 1099.8	21 min.	4μ layer
LS64	"	"	"	S 1050 R 960 - 965	15 hours	Garnet epi + polycrystal growth Colorless whiskers Red orthoferrite
LS65	"	"	"	S 1150 R 998.2 - 1004.7	20 min.	11μ layer
LS71	"	17.9%	"	S 1150 R 953.8 - 958.8	60 min.	6μ layer
LS76	"	19.1	"	S 1155 R 10450 - 1049.4	40 min.	1μ layer specular

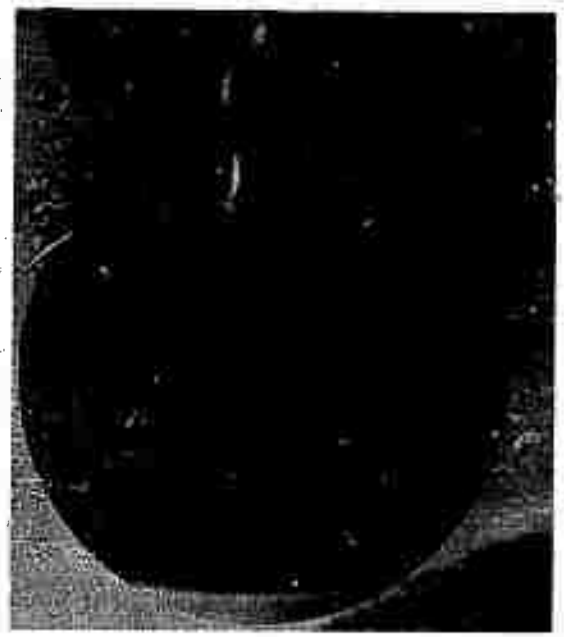

Figure 10. $EuEr_2Ga_{0.7}Fe_{4.3}O_{12}$ Epitaxial Layer After Growth. Platinum Wire Holder is at Top. Dark Regions are Adhered $BaO-BaF_2-B_2O_3$ Solvent (5X).

In most cases the epitaxial layers were faceted. Some of these layers, however, contained mobile magnetic domains, and subsequent polishing procedures increased the mobility of these domains. Typical domain structures are shown in Figures 11 and 12.

The extent of supersaturation in the 20.3 mole % solute growth runs is unknown, since the saturation temperature (Figure 3) is higher than the highest temperature attained for these runs. Layers with specular surfaces, which exhibited magnetic domains, were grown from a 19.1 mole % solute composition. The saturation temperature for this composition is ~ 1080-1090°C, and the best magnetic films were produced at growth temperatures of 1050°C (30-40° supercooling). These films, however, were very thin, typically ~1μ thick, even after 40 minutes in the growth solution.

Solvent adhered to the epitaxial layer and substrate holder in all cases as it was pulled out of the solution (see Figure 10), and when thicker than a few microns, caused severe cracking of the substrate as it cooled to room temperature. The solution adhesion problem is partially related to the viscosity of the solvent which appears to be higher than the $PbO-B_2O_3$ solvent at these temperatures. The higher the growth temperature, the lesser the amount of adhered solvent, and at 1050°C, by using a substrate holder such as that shown in Figure 10, the solvent was fluid enough to leave a large portion of the epitaxial layer uncracked. Adhered solvent was readily removed by etching in a 20% HNO_3 solution at ~80°C.

Figure 11. Serpentine Domain Pattern in $EuEr_2Ga_{0.7}Fe_{4.3}O_{12}$ Grown in $BaO-BaF_2-B_2O_3$ Solvent. Zero Bias Field, layer thickness 3μ, stripe width 5μ.

Figure 12. Bubble Domains Produced in the Layer Shown in Figure 11 by Application of 163 Oe Bias Field. Layer Thickness 3μ, Bubble Diameter 4μ.

2.2.3.2. Results of Growth in PbO-based Solvents

A series of growth runs in a $PbO-B_2O_3$ solvent was carried out for comparison with the epitaxial layers grown in the BaO-based solvents. Magnetic films of $Eu_2ErGa_{0.7}Fe_{4.3}O_{12}$; $GdY_{1.3}Yb_{0.7}Fe_{4.3}Ga_{0.9}O_{12}$, and $EuEr_2Ga_{0.7}Fe_{4.3}O_{12}$ were grown on {111} $Gd_3Ga_5O_{12}$ substrates by the dipping technique at temperatures ranging from 850 to 943°C. Most of the runs were performed at an isothermal growth temperature, while a few were carried out by rapid cooling techniques from 900-850°C. In all cases, the solvent contained 93.7 (mole)% PbO, and 6.3% B_2O_3. The solute concentration was varied from 6.66 (mole)% to 13.11%, and the rare earth concentration in the solute ranged from 20.23 to 10.13 (mole)%. Although epitaxial garnet layers could be grown from all these compositions, red orthoferrite platelets were also present on the epitaxial layer for all rare earth concentrations except the 10.13 mole %. In addition to these second-phase defects, triangular pits were often seen in the epitaxial layers, which usually did not extend all the way to the substrate surface. These defects trapped solution as the substrate was pulled out of the solvent after growth, and continuing growth under this region of trapped solution produced steps in the epitaxial layer. The number of such defects decreased as the rare earth concentration in the solute decreased. Specular surfaces on the epitaxial layers were obtained only if the initial solution temperature was above 1050°C, and the rough surfaces seen in other cases were attributed to competing growth reactions elsewhere in the growth crucible on nuclei that had not been completely dissolved during the initial high temperature period. Examples of epitaxial layers grown in this solvent are shown in Figures 13-16.

Figure 13. Serpentine Magnetic Domains in Epitaxially Grown $EuEr_2Ga_{0.7}Fe_{4.3}O_{12}$. Zero Bias Field, Layer Thickness 11μ, Stripe Width 7.5μ.

Figure 14. Effect of 137 Oe Magnetic Bias Field Applied to the Domains in Figure 15. Layer Thickness 11μ, Bubble Diameter 5μ .

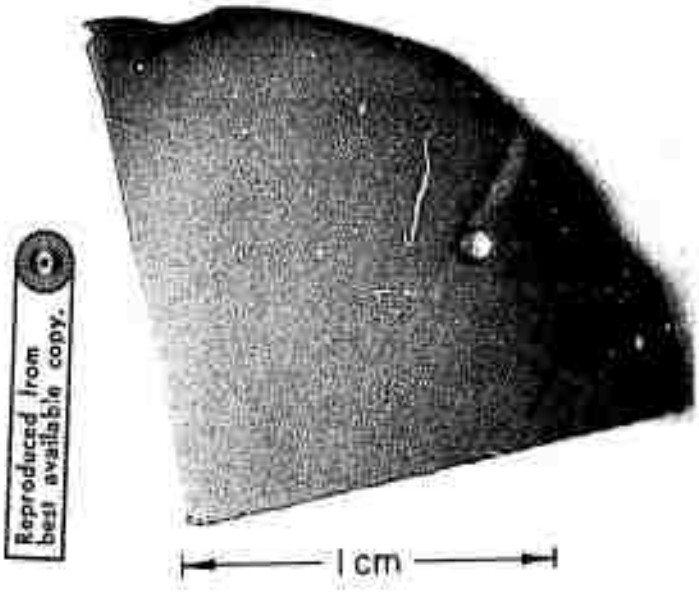

Figure 15. $GdY_{1.3}Yb_{0.7}Fe_{4.1}Ga_{0.9}O_{12}$ Epitaxial Layer Grown in $PbO-B_2O_3$ Solvent on {111} $Gd_3Ga_5O_{12}$ Substrate. Light Streak Above Hole is Caused by Uneven Growth Under Platinum Wire Substrate Holder.

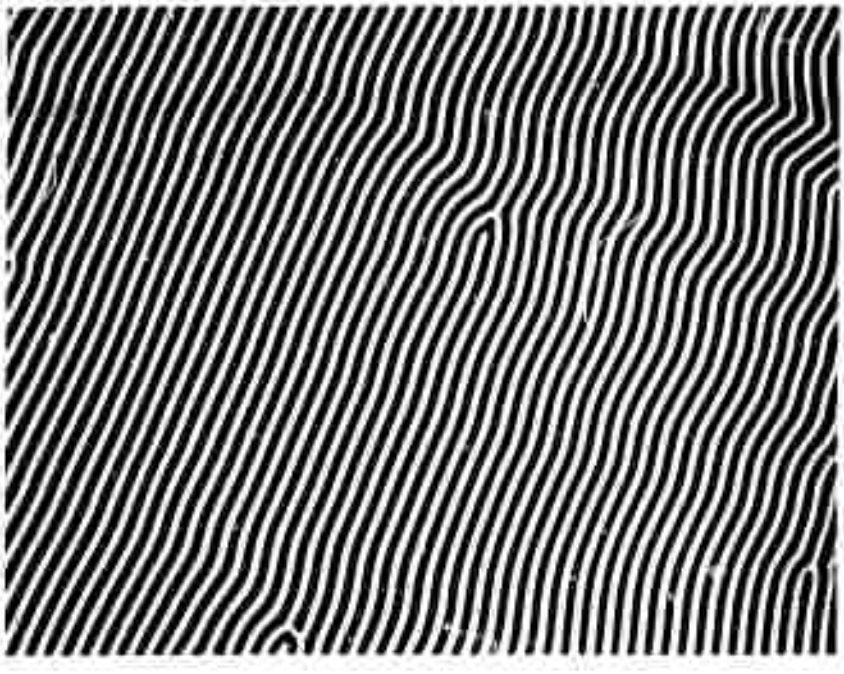

Figure 16. Serpentine Domains in Epitaxially Grown $GdY_{1.3}Yb_{0.7}Fe_{4.1}Ga_{0.9}O_{12}$. Layer Thickness 13μ, Stripe Width 5μ.

SECTION III

3.0. CHARACTERIZATION AND EVALUATION

3.1. Emission Spectrographic Analysis

Emission spectrographic analyses were performed on garnet epitaxial layers grown in BaO-based solvents to determine the amount of solvent incorporated into the garnet structure during growth. The garnets were prepared in several ways: (i) by grinding the substrate from an epitaxial layer greater than 20 microns thick, (ii) by sampling portions of the rare earth garnet which had not grown epitaxially on the substrate or (iii) by crushing substrate and epitaxial layer together in a mortar and pestle, followed by magnetic separation of the epitaxial portion. Each of these methods was followed by successive crushing and washing steps in hot 20% NHO_3, and finally sieving to produce a uniform grain size. The results did not differ significantly for any of these methods.

Barium content in $EuEr_2Ga_{0.7}Fe_{4.3}O_{12}$ epitaxial films as a function of growth parameters is shown in Table V, where it is seen that the impurity concentration is quite small and, in general, decreases with increasing temperature and decreasing growth rate. The data reflect both the solubility of barium with temperature as well as the growth rate effect upon both the equilibrium and interface distribution coefficients, since both are known to vary with temperature.[14] Consequently, it is difficult to extract equilibrium solubility data from this table.

3.1.2. Electron Microprobe Analysis

This analysis was performed to determine the respective amounts of the major constituents and the quantitative determination of impurities where

TABLE V

Solvent Impurity Content in Rare Earth Garnet Grown in $BaO-B_2O_3-BaF_2$ Solvent.

Run No.	Growth Temp. (°C)	Growth Rate (cm/sec)	Thickness (μ)	Barium† Content (wt. %)
LS53	947	1×10^{-6}	12μ	0.06
LS55	953	1.11×10^{-6}	10μ	0.054
SSG8	957	2×10^{-6}	6μ	0.042
LS64	962	-	Not Epitaxial	0.022
LS65	1000	9.17×10^{-7}	11μ	0.016
LS63	1095	3.3×10^{-7}	4μ	0.005

†These numbers represent upper limits to the barium content, since in some cases the analyzed specimens contained up to 50% Gd from the substrate and the numbers have been adjusted accordingly.

possible. Both qualitative (wavelength scan) and quantitative analyses were undertaken. Specimen FP12 (Table VIII) was selected for preliminary (qualitative) studies. Complete (three spectrometer) wavelength spectral scans were run for qualitative determination of all elements of atomic number 8 (oxygen) and higher. Detection limits were variable, particularly for the lighter elements, but were seldom less than 0.05 weight percent. Investigations were then made to determine the optimum analytical lines and instrument conditions for the quantitative analysis of elements detected in the spectral scans, Viz., Fe, Er, Ga, Eu, and Pb. Barium was also sought, but was not detected; oxygen was determined by difference.

The samples were analyzed on an ARL Model EMX-SM electron microprobe, utilizing a constant X-ray emergence angle of 52.5° and simultaneous digital readout from three X-ray spectrometers. An electron accelerating potential of 30 kV was used for all analyses. A 30-micron beam diameter was employed in order to partially reduce the effects of sample inhomogeneity at the micron level. Three ten-second counts were made on each of 5-to-8 points on each sample, the number of points examined depending on the apparent homogeneity of the sample. The analytical lines, dispersing crystals and standards are given in Tables VI and VII. Emitted X-ray intensities from each sample and standard were averaged and corrected manually for counting dead-time, drift and background. The corrected intensities were then further corrected for matrix errors (absorption, enhancement, ionization and penetration) using an IBM 360 computer with a modified version of the MAGIC Program.[18]

TABLE VI

Analytical Lines and Dispersing Crystals used for Each Element.

Element	Spectral Line	Wavelength	Order	Dispersing Crystal
Fe	K_α*	1.937	1	LiF
Er	L_{α_1}	1.784	2	LiF
Ga	K_α*	1.341	1	LiF
Eu	L_α	2.210	1	LiF
Ba	L_{α_1}	2.775	1	LiF
Pb	M_{α_1}	5.285	1	ADP

*Weighted average of K_{α_1} and K_{α_2}.

TABLE VII

Standards used for all Elements Except O.

Element	Standards
Fe	Fe_2O_3, $Er_3Fe_5O_{12}$
Er	Er_2O_3, $Er_3Fe_5O_{12}$
Ga	GaAs, $Gd_3Ga_5O_{12}$
Eu	Eu_2O_3, $Eu_3Fe_5O_{12}$
Ba	$BaSO_4$, $BaTiSi_3O_9$
Pb	PbS

The results (in atomic percent) are given in Table VIII. The distribution coefficients for Ga in octahedral and tetrahedral sites, and Eu in dodecahedral sites were derived from the microprobe data according to the ratios $\alpha_{Ga} = \frac{(Ga/Ga + Fe)\ crystal}{(Ga/Ga + Fe)\ solution}$ [7] and $\alpha_{Eu} = \frac{(Eu/Eu + Er)\ crystal}{(Eu/Eu + Er)\ solution}$, where Ga, Fe, Eu and Er are mole fractions. α_{Ga} and α_{Eu} are given in Table IX. These distribution coefficients are complex functions of temperature, growth rate, boundary layer thickness and initial gallium concentration in the solution (which varied slightly from run to run). α_{Eu} is nearly unity for a wide variety of growth conditions in both PbO-based and BaO-based solvents. α_{Ga} is nearly unity in the BaO-based solvents and varies little with temperature, while it ranges from 1.585 to 2.279 in the PbO-B_2O_3 solvent, depending upon growth parameters. This material parameter is thus much easier to control in the BaO-B_2O_3-BaF_2 solvent than in PbO-based solvents.

The variation of lead incorporation with growth rate is shown in Figure 17. This effect is probably caused by a combination of an increase in the lead distribution coefficient and an increase in the amount of micro-inclusions of solvent with growth rate, since these effects are indistinguishable by electron microprobe analysis.

3.2. Lattice Parameter Determinations

In order to determine the amount of lattice parameter mismatch between epitaxial layers and substrates, the lattice parameters have been measured on a number of samples by either powder pattern or single crystal techniques.

TABLE VIII

Compositions of the Epitaxial Layers

(Atomic percent)‡

	Growth Run Number††						
	FP11	FP12	LS15	LS19	LS27	LS55*	LS65*
Eu	4.8	4.9	9.3	9.4	5.3	5.5	5.3
Er	10.0	10.1	5.1	5.3	9.4	9.6	9.7
Fe	21.7	21.8	21.2	21.5	21.7	21.6	21.9
Ga	3.18	3.23	3.56	3.72	3.48	3.34	3.70
O	60.3	60.0	60.6	59.5	59.7	60.0	59.4
Ba	n.d.†	n.d.	n.d.	n.d.	n.d.	n.d.	n.d.
Pb	0.04	n.d.	0.20	0.60	0.40	n.d.	n.d.

*These two epitaxial layers were grown from the BaO-based solvents; all others were from the PbO-based solvents.

†These impurities were not detected. The limits of detection are 500 ppm and 300 ppm by weight for Pb and Ba, resepctively.

††Growth data for these runs are shown in Table IX.

‡ Estimated error limit ±2% of indicated value.

TABLE IX

Growth Data and Distribution Coefficients of Europium and Gallium

Sample	α_{Ga}	α_{Eu}	Garnet Composition (from Table VIII)	Solvent	Growth Temp. (°C)	Thickness (μ)	Average Growth Rate (cm/s)
FP11	2.279	0.963	$Eu_{0.97}Er_{2.03}Ga_{0.64}F_{4.36}O_{12}$	$PbO-B_2O_3$	874	4	6.7×10^{-7}
FP12	2.287	0.971	$Eu_{0.98}Er_{2.02}Ga_{0.64}Fe_{4.36}O_{12}$	$PbO-B_2O_3$	944	3.2	6.6×10^{-7}
LS15	1.585	0.971	Eu 1.9 Er 1.1 Ga 0.72 Fe 4.28 O 12	PbO-B 0 2 3	900 → 850 @2.7°C/min.	13	1.21×10^{-6}
LS19	1.626	0.964	Eu 1.9 Er 1.1 Ga 0.74 Fe 4.26 O 12	$PbO-B_2O_3$	900 → 850 @5.5°C/min.	14.4	2.67×10^{-6}
LS27	1.816	1.058	Eu 1.08 Er 1.92 Ga 0.7 Fe 4.3 O 12	PbO-B 0 2 3	900 → 850 @4.5°C/min.	11	1.53×10^{-6}
LS55	0.961	1.058	Eu 1.09 Er 1.91 Ga 0.67 Fe 4.33 O 12	BaO-B 0 -BaF 2 3 2	953	10	1.11×10^{-6}
LS65	1.039	1.110	Eu 1.06 Er 1.93 Ga 0.72 Fe 4.28 O 12	$BaO-B_2O_3-BaF_2$	1000	11	9.17×10^{-6}

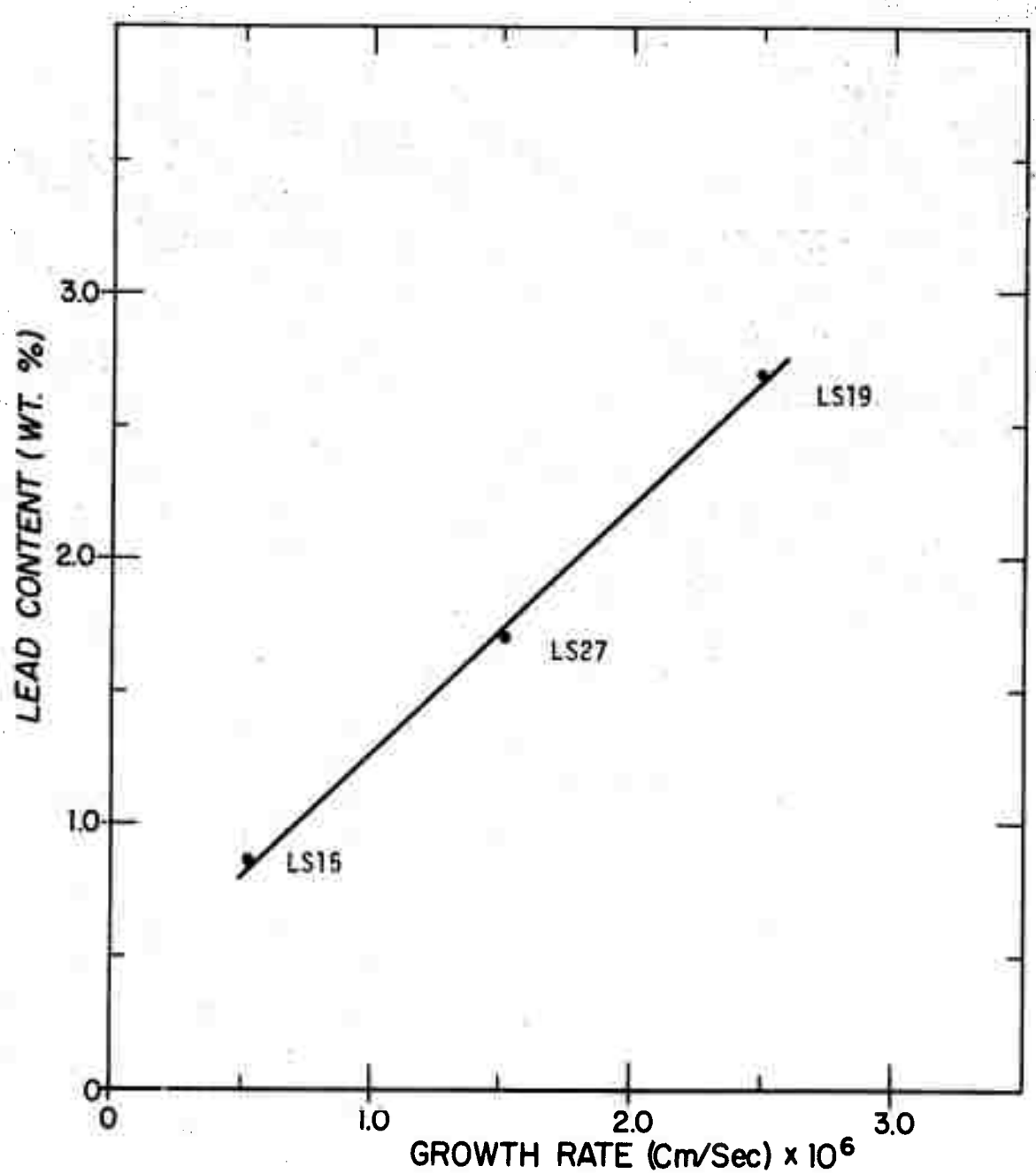

Figure 17. The Growth Rate Dependence of Lead Content in Garnet Epitaxial Layers Grown by the Cooling Technique from 900 to 850°C.

For the powder diffraction pattern the material was ground to a very fine powder (<0.04u), and rolled into a thin rod ~0.2 mm in diameter in a nondiffracting binder. After correcting the Debye-Scherrer data for film shrinkage, the lattice parameters were calculated from the diffraction lines from the back reflection region. These values were treated analytically to derive a linear experession based on the Nelson-Riley function[19]

$$\left(1/2 \left[\frac{\cos^2\theta}{\sin\theta} + \frac{\cos^2\theta}{\theta} \right] \right)$$

which allows extrapolation to $\theta = 90°$ where all of the systematic errors become negligible. The data were fitted to the expression by a least squares treatment to minimize the effect of random observational errors. The results of the powder pattern analysis are given in Table X.

The single crystal technique utilized a standard X-ray diffractometer fitted with either a scintillation counter or a lithium drifted silicon detector. Essential features of this method are (i) exact alignment of the tube, goniometer and single crystal sample, and (ii) the use of a beam slit with extremely low divergence. This same slit is then used in the measurement of the diffracting angles of different orders of a crystal plane. The goniometer is positioned to the true $2\theta = 0$ position using a beam alignment slit of 0.10 - 0.005°, a 0.4° scatter slit, and a 0.01° receiving slit with the zero alignment gauge placed in the center of the diffracting circle. The take-off angle of the tube is set at 2° or 3°, and the tube position adjusted to five maximum intensity readings on the detector. When proper alignment

TABLE X

Lattice Parameters of $Gd_3Ga_5O_{12}$ Substrates

AIRTRON			UNION CARBIDE		
Substrate No.	Powder Method	Single Crystal	Substrate No.	Powder Method	Single Crystal
5124004-002-A1	12.384 ±0.001		UC-A1	12.381 ±0.001	
5146-8292-01-A4-1	12.381 ±0.002		UC-2	12.378 ±0.002	
5146-8292-01-A4-48	12.379 ±0.002		T2-GGG-36-UC810	12.383 ±0.001	
			T2-GGG-37-UC818	12.385 ±0.002	12.388 ±0.002
5146-8292-01-A4-4	12.383 ±0.002	12.387 ±0.002	UC-A14		12.383 ±0.002
			UC-5		12.382 ±0.002
			T2-GGG-37-UC-B21		12.383 ±0.002

is achieved, the increase in intensity caused by changing from a receiving slit of 0.001" to 0.005" is no more than 25%, and removal of the zero alignment gauge does not result in a shift of the $2\theta = 0$ position as determined by scanning through the main beam.

Three peaks, the Cu $K_{\alpha 1}$, $K_{\alpha 2}$ and K_{β}, were measured for the (888) reflection for both the substrate and the epitaxial layer where possible. The results are given in Tables X and XI. In one case (LS27), the epitaxial layer was too thick to allow diffraction from the substrate, but for the majority of cases, a value could be determined for both. From these measurements, a linear plot of the lattice parameter for each peak versus the cot $\theta \cdot \cos\theta$ of the respective angle was derived, and extrapolated to $2\theta = 180°$ (where systematic errors such as absorption, misalignment of the instrument, use of a flat specimen, and vertical divergence become negligible) to determine the lattice parameter.

Variation in the $Gd_3Ga_5O_{12}$ substrate lattice parameters shown in Table X may be caused by variations in the gadolinium/gallium stoichiometry in the cation sublattice, which could be introduced by variations in Czochralski growth parameters, such as the melt stoichiometry, crystal rotation rate, pulling rate and the oxygen partial pressure above the melt. A similar variation in lattice parameter was found in $Y_3Ga_5O_{12}$ which is closely related to $Gd_3Ga_5O_{12}$.[19] In this case, Y^{3+} is substituted for Ga^{3+} on octahedral sites. This substitution expands the lattice from 12.274Å for the stoichiometric case to 12.438Å for the compound with the formula $Y_{3.74}Ga_{4.26}O_{12}$.

The data in Table XI reflect changes in lattice parameter due to the Eu/Er ratio[4] as well as a possible increase in lattice parameter caused by

TABLE XI

Lattice Parameters of Epitaxial Garnets

Sample	Solvent	X in $Eu_xEr_{3-x}Fe_{4.3}Ga_{0.7}O_{12}$	Amount of Pb(wt%)	Lattice Parameters		
				Substrate	Epitaxial Layer	Δa
FP16	$PbO-B_2O_3$	~1	N.A.	12.383 ±0.002	12.410 ±0.002	0.027
LS27	"	1.08*	1.70	(12.383)†	12.411 ±0.002	(0.028)†
LS15	"	1.93*	0.85	12.383 ±0.002	12.476 ±0.002	0.093
LS19	"	1.92*	2.50	12.383 ±0.001	12.480 ±0.002	0.097
LS23	$BaO-B_2O_3$ BaF_2	~2	N.A.	12.382 ±0.002	12.457 ±0.002	0.075

*These values were derived from microprobe data, others are estimated from solution composition.

†Estimated values.

N.A. Not Analyzed

lead incorporation in the lattice. The latter factor is indicated by a 0.004Å increase (which is however, within experimental error) in the epitaxial layer lattice parameter between LS15 and LS19, as the lead content increased from 0.85 to 2.50 wt. %. In these runs, however, the growth rate also increased, and the lead content may reside in microscopic inclusions of solvent in the layer as discussed in Section 3.1.2. Giess et al.[8] report an increase in lattice parameter of ~0.01Å for a similar increase in lead content. The lead was not detectable (and is presumed <0.05 wt. %) for the epitaxial layer grown at 944°C (FP12). It is interesting that the layer grown in the BaO-based solvent (LS23) also has a significantly lower lattice parameter. This epitaxial layer contained < 0.03 wt. % Ba^{2+}. The $Gd_3Ga_5O_{12}$ substrate lattice parameter does not appear to be affected by the epitaxial growth as reported by Shick et al.[4]

3.3. Magnetic Measurements

3.3.1. Mobility and Coercive Force Measurements

Local variations in coercive force in the magnetic films were monitored by visual observation of the response of the magnetic domains to an AC modulation (~ 20 Hz) of an applied magnetic bias field. The domain walls move in response to the AC field except where they are pinned by defects in the film as shown in Figure 18 . This technique was used to provide a qualitative check of the quality of the epitaxial layer.

Apparatus was constructed for the determination of mobility and coercivity by optical techniques and initial measurements were made. In this technique, the coercive force is measured by the application of an oscillating magnetic field to a magnetic film having the stripe domain configuration. Transmitted polarized light is modulated by the domain wall motion, and the signal is detected by a photomultiplier tube, then demodulated by a lock-in amplifier. As the amplitude of the oscillating magnetic field is decreased, the oscillating light intensity also decreases. The coercive force is found by the x-axis intercept of the curve of AC light intensity versus magnetic field. Preliminary results indicate that the coercive force is lower in films grown in the BaO-based solvent than in the PbO-based solvent, but quantitive data have not yet been obtained.

The mobility is measured by determining the variation of domain wall position with time after a step change in applied magnetic field is made. Figure 19 shows the apparatus used for detecting domain wall motion by the change in light intensity of a polarized He-Ne laser beam reaching the

Figure 18. Magnetic Domains Moving in Response to AC Modulation (19 Hz) of the 20 Oe Magnetic Bias Field Except Where Pinned at Defect (200X).

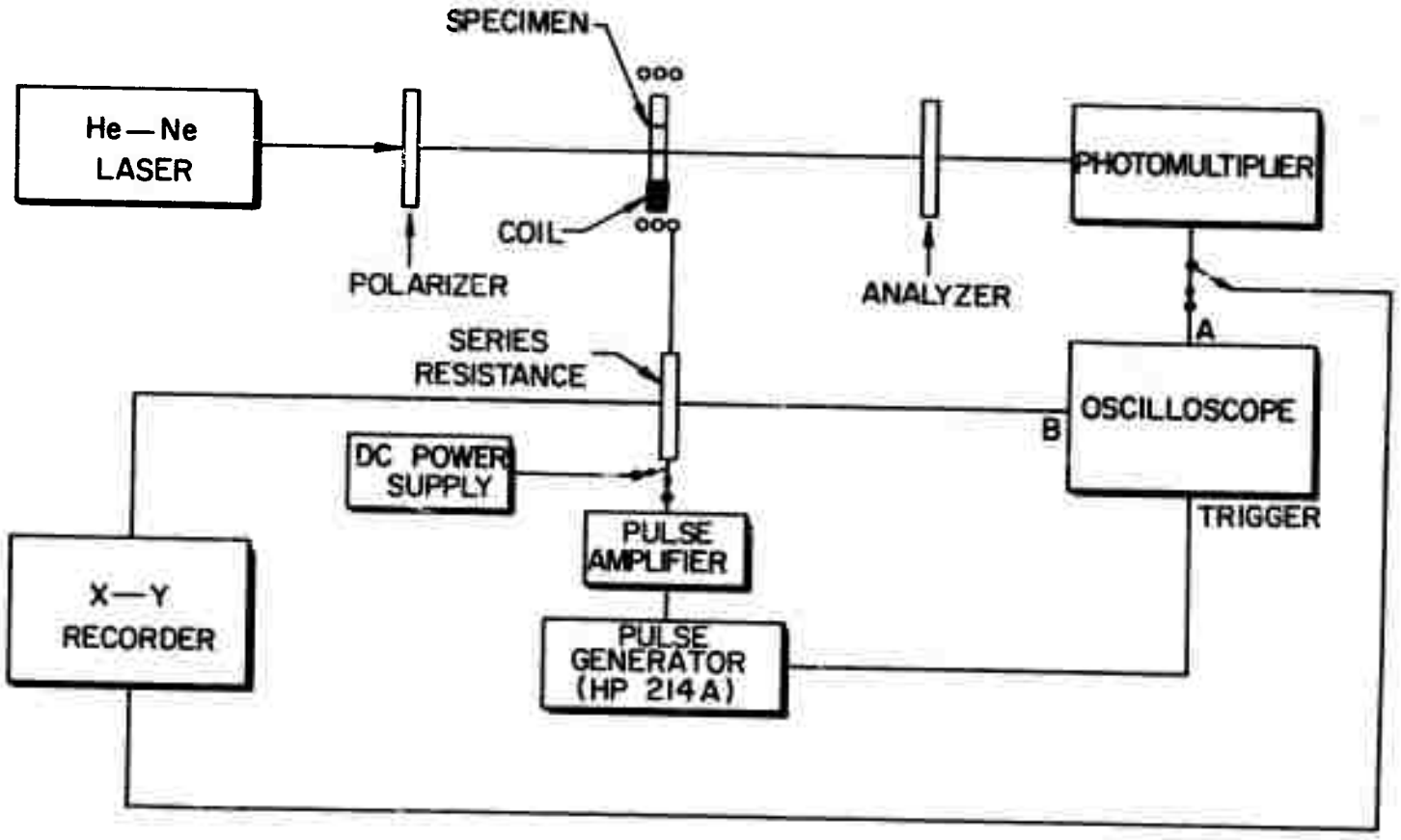

Figure 19. Schematic of Apparatus for Coercivity and Mobility Measurements.

photomultiplier tube. Data are derived from the rate at which light intensity reaches its equilibrium value. To obtain a satisfactory signal to noise ratio, it is necessary to integrate many repetitions of the applied square wave pulse, which is done by using the sampling oscilloscope as a boxcar integrator. Mobility measurements will be made using these techniques during the next report period.

3.3.2. Magnetization and Anisotropy Measurements

A recently constructed torque magnetometer has been used for measurements of the saturation magnetization and anisotropy constants of the epitaxial layers grown in this program. To date, initial measurements have been made on LS27 and FP12 and the results are as follows:

	$4\pi M_s$ (gauss)	H_k (oersted)
LS27	243 ±10	5316 ±100
FP12	213 ±10	8426 ±100

These values are higher than the optimum values for these garnets and may reflect stress as well as growth induced anisotropy in the layer.

3.3.3. Curie Point Measurements

A hot stage microscope has been set up for Curie point measurements in the magnetic films in order to determine the gallium/iron ratio in the epitaxial layers. The Curie point of LS27 was found to be ~ 195°C by monitoring the temperature range in which the domains faded entirely

from view in the polarizing microscope and in which an entirely new domain pattern appeared upon cooling. If the Curie point of $EuEr_2Fe_5O_{12}$ is assumed to be 560°K (by linear interpolation between the end members), and if gallium lowers the Curie point in the same fashion as in YIG, this Curie temperature of 195°C predicts the garnet composition $EuEr_2Ga_{0.7}Fe_{4.3}O_{12}$, which is nearly identical to the microprobe results. This technique is hampered by the fact that the Curie transition actually occurs over a range of temperatures and it is difficult to visually detect the temperature at which the domains vanish. In addition, for materials with high magnetostriction constants, such as $GdY_{1.3}Yb_{0.7}Fe_{4.1}Ga_{0.9}O_{12}$, the stress induced anisotropy may vanish before the Curie point is reached, leading to anomalous results.

SECTION IV

4.0. CONCLUSIONS

Quasi steady-state liquid phase epitaxial growth of the magnetically uniaxial mixed rare earth garnets in the $BaO-B_2O_3-BaF_2$ solvent has been demonstrated. Comparison of LPE growth of the same garnets in a $PbO-B_2O_3$ solution reveals strengths and weaknesses of each of these solvents. The PbO-based solvents are quite volatile and readily lose PbO at typical crystal growth temperatures exceeding 900°C. The freezing point of this solvent is quite low, and the garents can be successfully grown at temperatures as low as 800°C, where the PbO volatilization is much less severe; however, the Pb distribution coefficient in the garnet increases rapidly with decreasing temperature, so that as much as 3 wt. % Pb may be incorporated into the epitaxial layer at 850°C, compared to less than 0.05 wt. % at crystal growth temperatures of 940°C.

The Ba content in layers grown in BaO-based solvents ranges from 0.05 wt.% for growth temperatures of ~950°C to 0.005 wt. % at ~1100°C, and therefore should not perturb the magnetic properties of the layer. The BaO-based solvent is too viscous for LPE growth below 1000°C, but is nonvolatile at temperatures as high as 1400°C, and thus presents no serious barrier to high temperature LPE growth. However, there are two difficulties arising from excessive crystal growth temperature of the rare earth garnets: (i) the larger amounts of strain resulting from the difference in thermal expansion coefficients of epitaxial layer and substrate, and (ii) the possible loss of growth induced anisotropy at higher temperatures. The major problem associated with the BaO-based solvent is its greater tendency to adhere to the epitaxial layer after growth, which then induces cracking

upon cooling to room temperature. This problem can probably be alleviated by growing at temperatures above 1050°C, where the solvent is fluid enough to run off the layer, and by using a more sophisticated growth scheme than the simple dipping technique, such as a holder which can rotate a horizontally held substrate to spin off the growth solution. The rare earth garnets are more soluble in the BaO-based solvent than in the PbO-based solvent, and are congruently saturating in the former solvent, which represents a slight advantage.

The microprobe analyses indicate that α_{Eu} is close to unity in both solvents at different growth rates and at different temperatures, which one might expect since there is only a 2.14% difference in ionic radius between Eu^{3+} and Er^{3+}. For Fe^{3+} and Ga^{3+}, on the other hand, where the difference in ionic radius is 32.4%, α_{Ga} has been found to vary significantly with growth rate and growth temperature in the $PbO-B_2O_3$ solvent but not in the BaO-based solvent, an advantage when there are temperature excursions in the growth solution.

The substrate lattice parameter does not appear to be affected by the presence of the epitaxial layer, even for differences in lattice parameter of 0.097 A, and there does not seem to be a significant difference in this respect between the PbO and BaO-based solvents.

More experimentation is needed with the BaO-based solvent, particularly at higher growth temperatures with more sophisticated substrate holders, to fully utilize its advantages in LPE growth of the bubble garnets.

REFERENCES

1. A. H. Bobeck, R. F. Fischer and J. L. Smith, presented at 17th Conference on Magnetism and Magnetic Materials, November 1971.

2. R. A. Burmeister, T.L. Felmlee and R. Hiskes, Final Technical Report, Magnetic Rare Earth Compounds, Contract No. DAAH01-70-C-1106, Program Code No. 0D10, June 1971.

3. J. W. Nielsen, Met. Trans. 2, 625 (1971).

4. L. K. Shick, J. W. Nielsen, A. H. Bobeck, A. J. Kurtzig, P. C. Michaelis and J. P. Reekstin, Appl. Phys. Letters 18, 89 (1971).

5. R. C. Linares, R. B. McCraw and J. B. Schroeder, J. Appl. Phys. 36, 2884 (1965).

6. R. C. Linares, J. Cryst. Growth 3,4, 443 (1968).

7. E. A. Giess, B. E. Argyle, B. A. Calhoun, D. C. Cronemeyer, E. Klokholm, T. R. McGuire and T. S. Plaskett, to be published.

8. E. A. Giess, B. E. Argyle, D. C. Cronemeyer, E. Klokholm, T. R. McGuire, D. F. O'Kane, T. S. Plaskett and V. Sandagopan, presented at 17th Conference on Magnetism and Magnetic Materials, November 1971.

9. D. M. Heinz, P. J. Besser, P. E. Elkins, H. L. Glass, J. E. Mee and L. A. Moudy, Technical Report AFML-TR-71-126, June 1971.

10. R. Zeyfang, J. Appl. Phys. 41, 3718 (1970).

11. D. M. Heinz, P. J. Besser, J. M. Owens, J. E. Mee and G. R. Pulliam, J. Appl. Phys. 42, 1243 (1971).

12. J. E. Mee, G. R. Pulliam, D. M. Heinz, J. M. Owens and P. J. Besser, Appl. Phys. Letters 18, 60 (1971).

13. J. E. Mee, P. J. Besser and F. A. Pizzarello, Technical Report AFAL-TR-70-194, Sept. 1970.

14. D. Elwell and B. W. Neate, J. Mat. Sci. 6, 1499 (1971).

15. M. Robinson, A. H. Bobeck and J. W. Nielsen, IEEE Trans. on Mag., Sept. 1971.

16. R. C. Linares, J. Am. Cer. Soc. 45, 307 (1962).

17. H. J. Levinstein S. Licht, R. W. Landorf and S. L. Blank, to be published.

18. J. W. Colby, MAGIC, Version IV, A computer Program for Quantitative Electron Microprobe Analysis, a Bell Telephone Laboratory Report, Allentown, Pa., Aug. 1971.

19. L. V. Azaroff and M. J. Buerger, "The Powder Method of X-ray Crystallography," McGraw Hill Book Co., Inc., New York, 1958.

20. S. Geller, Z. Krist. 125, 1 (1967).

REFERENCES for TABLE III

1. A. H. Bobeck, E. G. Spencer, D. H. Smith, and L. G. Van Uitert, paper presented at Intermag. Conference, April 1971, Denver, Colorado.

2. L. G. Van Uitert, W. A. Bonner, W. H. Grodkiewicz, Miss L. Pictroski and G. J. Zydzik, Mat. Res. Bull. 5, 825 (1970).

3. L. K. Shick, J. W. Nielsen, A. H. Bobeck, A. J. Kurtzig, P. C. Michaelis and J. P. Reekstin, Appl. Phys. Letters 18, 89 (1971).

4. E. A. Giess, B. E. Argyle, B. A. Calhoun, D. C. Cronemeyer, E. Klokholm, T. R. McGuire and T. S. Plaskett, to be published in Mat. Res. Bull. Nov. 1971.

5. R. Wolfe, J. C. North, R. L. Barns, M. Robinson and H. J. Levinstein, Appl. Phys. Letters 19, 298 (1971).

6. B. A. Calhoun, E. A. Giess and L. L. Rosier, Appl. Phys. Letters 18, 287 (1971).

7. E. A. Giess, B. A. Calhoun, E. Klokholm, T. R. McGuire and L. L. Rosier, Mat. Res. Bull 6, 317 (1971).

8. D. M. Heinz, P. J. Besser, J. M. Owens, J. E. Mee and G. R. Pulliam, J. Appl. Phys. 42, 1243 (1971).

9. D. M. Heinz, P. J. Besser, P. E. Elkins, H. L. Glass, J. E. Mee and L. A. Moudy, Technical Report AFML-TR-71-126, Air Force Materials Laboratory. Air Force Systems Command, Wright-Patterson Air Force Base, June 1971.

10. H. J. Levinstein and R. W. Landorf, Intermag. Conference, Denver, Colorado, April 1971.

11. A. H. Bobeck, R. F. Fischer and J. L. Smith, to be published.